

Properties of ultra-high performance concrete using optimization of traditional aggregates and pozzolans



Ariful Hasnat*, Nader Ghafoori

Department of Civil and Environmental Engineering and Construction, University of Nevada, Las Vegas, 4505 Maryland Parkway, Box 454015, LV 89154-4015, United States

HIGHLIGHTS

- Conventional fine aggregates and pozzolans can be used to produce UHPCs.
- Overall, ternary blend UHPCs containing silica fume and fly ash exhibited highest bulk properties.
- Inclusion of steel fibers significantly improved splitting-tensile and flexural strength of the studied UHPCs.
- Drying shrinkage of the plain UHPCs decreased with increases in aggregate-to-cementitious materials ratios.
- An increase in steel fiber content significantly improved post-peak retention capacity.

ARTICLE INFO

Article history:

Received 29 November 2020
Received in revised form 18 May 2021
Accepted 6 June 2021
Available online 17 June 2021

Keywords:

Conventional fine aggregate
Ultra-high performance concrete
Bulk properties
Cementitious materials
Steel fiber
Drying shrinkage

ABSTRACT

The properties of ultra-high performance concretes (UHPCs) made with traditional fine aggregates, different cementitious materials types and combinations, and varying steel fiber contents and shapes were studied. In the first phase, a total of 78 UHPCs were used to assess their compressive and splitting-tensile strengths, and drying shrinkage, which led to identifying 40 optimized mixtures for the second phase of the investigation for which their compressive, splitting-tensile, and flexural strength, modulus of elasticity, load-deflection response, and drying shrinkage properties were obtained. The outcome of this study revealed that the optimized UHPCs displayed excellent bulk properties and dimensional stability. Amongst the utilized cementitious materials combinations, UHPCs made with the combined silica fume and class F fly ash, as a partial replacement of cement, performed the best, whereas the companion mixtures incorporating only class F fly ash exhibited the contrary. A clear strain hardening and softening was observed in the load-deflection response of steel fiber-reinforced UHPCs. Due to better steel to concrete surface adhesion, straight steel fibers had a more positive influence on the mechanical properties and dimensional stability of the studied UHPCs when compared to those of the hooked fibers. Overall, this experimental study supports that, with proper gradations and proportioning, traditional fine aggregates can be used as an effective substitute for the expensive filler materials used for production of the proprietary UHPCs without compromising their mechanical properties and dimensional stability.

© 2021 Elsevier Ltd. All rights reserved.

1. Introduction

In recent years, the utilization of advanced chemical admixtures and fibers; specialized aggregates with excellent packing density; very high binder content; low water-to-cementitious materials ratio; and customized mixing and curing has led to the development of ultra-high performance concrete (UHPC) [1-8]. According to ACI 239R [9], "Ultra-high performance concrete (UHPC) is a class of advanced cementitious materials with greater strength, tensile ductility, and durability properties when compared to conven-

tional or even high-performance concrete. UHPC is limited to concrete that has a minimum specified compressive strength of 22,000 psi (150 MPa) with specified durability tensile ductility and toughness requirements; fibers are generally included to achieve specified requirements." In ASTM C1856 [10], it is mentioned that, UHPC should have "specified compressive strength of at least 120 MPa, with nominal maximum size aggregate of less than 5 mm and a flow between 200 and 250 mm." UHPC provides the following advantages over conventional concrete:

* Corresponding author.

E-mail addresses: hasnat@unlv.nevada.edu (A. Hasnat), nader.ghafoori@unlv.edu (N. Ghafoori).

- (i) The very high compressive, tensile, and flexural strengths, and modulus of elasticity of UHPC results in significant reduction in the sectional size of the concrete members, which saves floor space and reduces structural dead load. Blais and Couture [11] mentioned that UHPC members may weigh only one-third to one-half of corresponding conventional concrete members.
- (ii) Superior ductility and energy absorption provide greater reliability even under extreme conditions, such as earthquakes or blasts. Moreover, fibers inside UHPC enable the concrete to sustain structural integrity towards tensile load after first cracking, by bridging cracks and transferring the load across the cracks [12].
- (iii) The superior durability of UHPC leads to a long service life with reduced maintenance. UHPC is nearly impermeable, allowing almost no carbonation nor chloride or sulfate penetration [13]. Bonneau et al. [14] documented that only 26% of cement hydration is required for UHPC to achieve discontinuous capillary pores.
- (iv) A significant amount of unhydrated cement in the hardened UHPC provides a self-healing potential under cracking conditions [15].
- (v) The absence of coarse aggregate in UHPC allows for high quality surface finishes [11].
- (vi) The circulation of stray current through conventional steel reinforcement is known to cause accelerated corrosive damage to steel. Unlike conventional steel reinforcement in concrete, fiber-reinforced UHPC does not usually have a continuous conductive path for an electric current [16].

Some suggestions of drawbacks associated with the use of UHPCs reported in the literature are:

- (i) Only a few proprietary blends have been used by different researchers in the assessment of UHPC properties. The utilization of a very high amount of silica sand, steel fibers, chemical admixtures, and silica fume in proprietary UHPCs make the production costs of such mixtures about 10 to 20 times higher than conventional concrete [8,17,18].
- (ii) Under normal curing condition, UHPCs are susceptible to higher autogenous and drying shrinkage due to their higher amounts of cementitious materials and high range water reducing admixture [19].
- (iii) High shear mixers are needed to properly batch UHPC's ingredients. This kind of mixers may not be available at construction sites [20]. Additionally, specific procedures maybe needed including the use of ice cubes instead of water to provide the shearing action and to reduce heat of hydration and mixing time.
- (iv) There is lack of design codes for using UHPCs [1].

The first structural application of UHPC was in 1997, when UHPC was used to construct a pre-stressed hybrid pedestrian bridge in Sherbrooke, Canada [21]. After that, applications of UHPC were successfully demonstrated in several countries [22,23]. However, the widespread use of UHPC is still limited due to high initial production cost. A number of researchers have tried to compensate for the very high production costs of UHPCs by using different materials and methods (Table 1). Karim et al. [13] used masonry sand as a replacement for expensive quartz sand, while Arora et al. [24] used coarse and fine aggregates collectively to reach a compressive strength of 150 MPa. Yang et al. [25] reduced the total cost of UHPC by utilizing supplementary cementitious materials, such as fly ash and ground granulated blast-furnace slag (GGBS), as a partial replacement for Portland cement. Alsalman et al. [26] reported that more than 10% silica fume content, as a partial

Table 1
Studies on UHPCs with conventional aggregates.

Reference	Materials used as aggregates	Properties evaluated ^a
Sobuz et al. [60]	Fine aggregate: washed river sand, mined sand, manufactured sand, and granulated lead smelter slag; Coarse aggregate: crushed bluestone	Compressive strength (121–153 MPa); elastic modulus (10.2–40.9 GPa); strain at peak stress (0.00426–0.0091)
Meng et al. [30]	Missouri river sand, masonry sand	Compressive strength (120–135 MPa); splitting-tensile strength (10–14 MPa); flexural strength (20–24 MPa); elastic modulus (46–53 GPa); drying shrinkage (56–600 $\mu\text{m}/\text{m}$)
Alsalman et al. [26]	Arkansas river sand, class C fly ash	Compressive strength (124.1–162.4); elastic modulus (36.9–45.9 GPa)
Karim et al. [13]	Conventional fine aggregate, masonry sand	Splitting-tensile strength (10.1–11.8 MPa); drying shrinkage (0.110–0.148%)

^a properties relevant to present study.

replacement of Portland cement, had a minimal effect on compressive strength, whereas other researchers emphasized using a high volume of silica fume to achieve the desired properties [27–29].

An essential constituent in UHPC is discontinuous fiber reinforcement. The inclusion of fiber is necessary to improve the ductility required for structural safety. Meng et al. [30] employed hybrid fibers, and evaluated the fresh and mechanical properties of non-proprietary UHPCs. When compared to conventional concrete, due to the presence of fiber reinforcement, UHPC has exhibited considerable tensile strength, even after first cracking [12]. Another study reported a profound improvement in flexural tensile strength corresponding to an increase in fiber content [31]. Máca et al. [32] used steel fiber and reported that the highest flexural strength is obtained when a 3% fiber volume is used. In another study, Yoo et al. [33] concluded that an increase in steel fiber content resulted in an improved elastic modulus up to 3% of fibers. Wille et al. [34] pointed out that twisted steel fibers led to lower tensile strength than straight steel fibers at elevated load rates. Yoo et al. [33] also found that straight fibers outperformed twisted/hooked fibers in flexural tensile strength performance. In contrast, other studies have reported better performance by twisted or hooked fibers in flexural/tensile strength performance, as compared to that of straight fibers [35,36].

In recent years, a number of researchers have conducted studies in optimization of UHPC's compositions with limited information available to date [13,26,30]. In particular, literature suffers from limited data on utilization of various supplementary cementitious materials in production of sustainable and cost-effective UHPCs. This paper aimed to investigate the role of different cementitious materials compositions and aggregate-to-cementitious materials ratios, as well as various steel fiber contents and shapes, on properties of the studied UHPCs. The investigated properties included compressive strength, splitting-tensile resistance, flexural strength, load–deflection response, flexural strain, elastic modulus, and drying shrinkage. The outcome of this investigation will add to the body of knowledge in utilization of locally available aggregates and different supplementary cementitious materials in production of UHPCs.

2. Experimental Program

This study was divided in two Phases. In the Phase I, various cementitious materials types and combinations, aggregate grada-

tions, water-to-cementitious materials ratios, and aggregate-to-cementitious materials ratios were evaluated to identify the optimized plain UHPCs. During Phase II of this study, the effects of steel fiber contents and shapes on the bulk properties and dimensional stability of the optimized UHPCs were investigated. As this study has two Phases (Phase I and II), all materials and method section explained at the Experimental Program Section, with the exception of mixture design of Phase II (as these mixtures were selected once Phase I was completed).

2.1. Materials

A quest for UHPC optimization using traditional aggregates was undertaken based on standard tests. In the production of the UHPCs, ASTM Type V Portland cement (C), class F fly ash (F), natural pozzolan (N), ground granulated blast-furnace slag (S), and silica fume (SF) were used as cementitious materials. Type V cement (with 4% C₃A) was selected to ensure the resistance against severe sulfate action. The chemical characteristics of the cementitious materials are presented in Table 2, and scanning electron microscopic (SEM) images are shown in Fig. 1. Fig. 2 represents the particle size distribution of the cementitious materials. Silica fume, slag, industrial (Class F fly ash), and natural pozzolans were used at different replacement levels of cement content. The natural pozzolan was sourced from a vitrified rhyolite as a silica-rich volcanic ash. Several investigators assessed the effect of steel fiber content (up to 3%) on properties of UHPCs [37–39]. In the Phase II of this study, two types of steel fibers (straight and hooked), with 13 mm length and 0.30 mm width (aspect ratio of 43) were used at the levels of 2 and 3% of the total concrete volume. The specific gravity of the steel fibers was 7.86 and met the minimum tensile strength requirement of ASTM A820 [40].

2.2. Selection of cementitious materials Combinations, w/cm, and HRWRA content

At first, 100% cement was batched at various water-to-cementitious materials ratios ($w/cm = 0.16–0.24$), and tested for flow to obtain the minimum water content required to achieve the minimum relative flow, as shown in Fig. 3a. A total of 30 combinations of cementitious materials (15 binary, 10 ternary, and four quaternary cementitious material compositions) were batched at various water-to-cementitious material ratios ($w/cm = 0.16–0.24$), and tested for flow to obtain the minimum water content (Fig. 3b) and HRWRA (polycarboxylate based) requirement of different binder combinations, in comparison with 100% cement. Based on the findings of flow test conducted in accordance with ASTM C230 [41], a total of 26 combinations of binders were selected with the water-to-cementitious materials ratio of 0.21. The correlation between the relative flow and required HRWRA to achieve the flow of 250 ± 25 mm is given in Fig. 3c.

Table 2
Chemical compositions of the Type V cement and pozzolanic materials.

Composition	Type V cement (%)	Class F fly ash (%)	Natural pozzolan (%)	GGBS (%)	Silica fume (%)
SiO ₂	21	59.93	71.0	31.0	94.72
CaO	62.4	4.67	2.3	43.64	–
Al ₂ O ₃	4	22.22	7.9	11.5	–
Fe ₂ O ₃	3.7	5.16	0.70	0.80	–
MgO	2.6	–	–	4.7	–
SO ₃	2.2	0.38	0.1	4.85	0.23
Na ₂ O + K ₂ O	0.54	1.29	7.5	–	0.47
Loss on Ignition (LOI)	2.0	0.32	3.4	0.30	2.82

2.3. Aggregate gradation

Two types of locally produced fine aggregates were used; their size gradation varied from 0.075 mm to 4.75 mm. To obtain the maximum packing density and minimum porosity, a uniquely-sized graded manufactured fine aggregate was determined and stored separately for each size gradation. Unit weight was measured for the graded aggregates at different distribution moduli (0.19–0.23), using the modified Andreasen and Andersen model, as shown in Fig. 4 [42]. The unit weight of the aggregates was determined as per ASTM C29 (rodding method) [43]. The modified Andreasen and Andersen particle packing model is based on the following equation:

$$P(D) = \frac{D^Q - D_{min}^Q}{D_{max}^Q - D_{min}^Q} \quad (1)$$

where, $P(D)$ represents the weight percentage of aggregate passing the sieve with size D ; D_{max} is the maximum particle size (μm); D_{min} is the minimum particle size (μm); and Q is the distribution modulus, which is related to the aggregate particle size. The maximum unit weight with minimum void percentage was obtained using the distribution modulus of 0.21. Sieve analysis of aggregate I, aggregate II, and the combined Andreasen and Andersen sizes (optimized curve) for the distribution modulus of $Q = 21$ is presented in Fig. 5. The combined fine aggregates had a specific gravity of 2.80, a fineness modulus of 2.92 and an absorption of 0.45%.

2.4. Mixture proportions of plain UHPCs

A total of 78 plain UHPC mixture compositions were selected to determine their compressive and splitting-tensile strengths and drying shrinkage. The aggregate-to-cementitious materials ratio (V_A/V_{cm}) plays an important part in the strength development of UHPC [13]. Most researchers selected a V_A/V_{cm} between 0.60 and 1.4 [2,30]. In this study, to observe the effect of the aggregate/cementitious materials ratio, the V_A/V_{cm} varied at 0.80, 1.0, and 1.2. For each V_A/V_{cm} , 26 cementitious compositions were investigated, which consisted of the control (C100), along with 13 binary, nine ternary, and three quaternary cementitious compositions. The unit contents of the selected UHPC constituents for various aggregate-to-cementitious materials ratios (V_A/V_{cm}) are given in Table 3. The water-to-cementitious materials ratio (w/cm) of 0.21 was kept constant for all mixtures. The actual water content of the UHPCs varied due to variation in the required HRWRA dosage to maintain uniform flowability.

2.5. Mixing, Sampling, Curing, and testing

Due to the high quantity of small-sized particles, coupled with the low water-to-cementitious materials ratio, and the addition of steel fibers (used in Phase II), a longer mixing time and higher energy were required for UHPC production as compared to tradi-

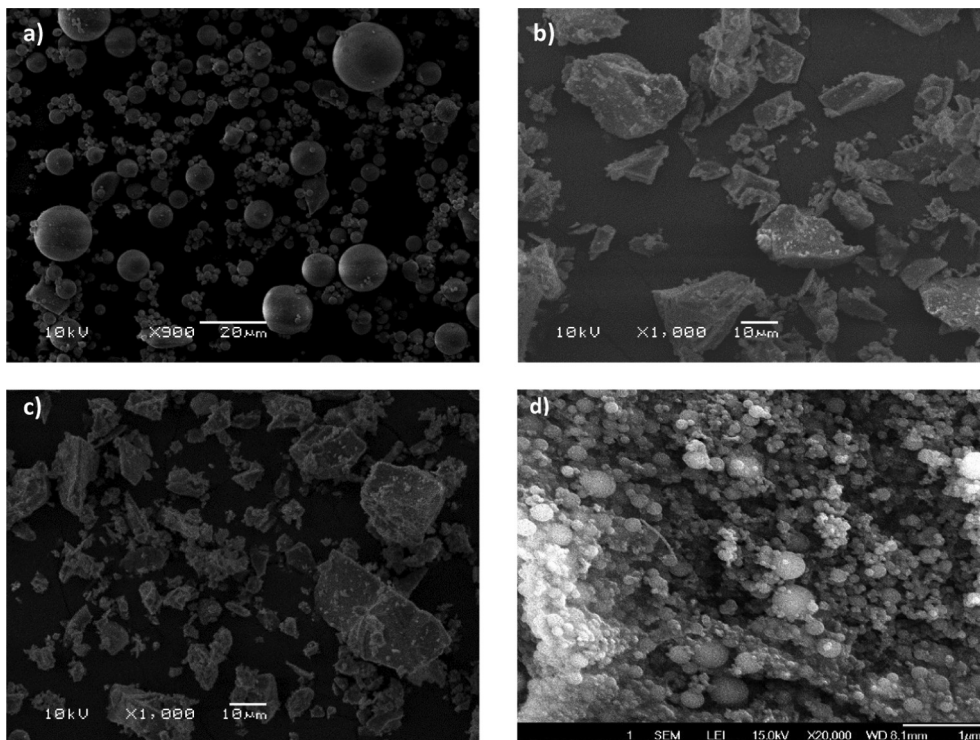


Fig. 1. Scanning electron microscopic (SEM) image of cementitious materials (a) class F fly ash, (b) natural pozzolan, (c) ground granulated blast-furnace slag, and (d) silica fume.

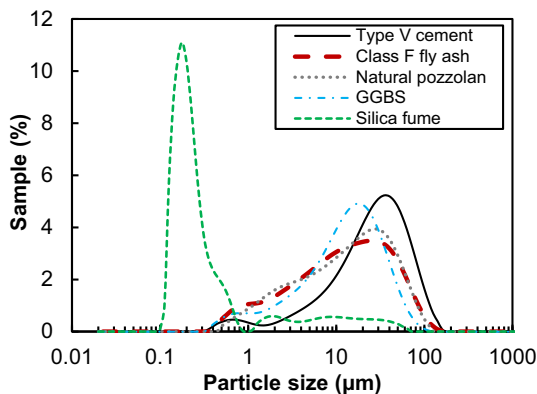


Fig. 2. Particle size distribution of cementitious materials.

tional concrete. The mixing time, mixing speed, mixing sequence, temperature, and relative humidity were closely monitored and uniformly maintained. The mixing sequence is shown in Fig. 6. The flow properties were evaluated according to the modified ASTM C230 (as all the UHPCs were self-consolidating, 25 drops of blow were skipped) before they were poured into cylinders and beam-shaped molds [13]. The specimens were kept for 24 h in a controlled-moisture curing room at 22 ± 3 °C and 95% relative humidity. After 24 h, the specimens were demolded and returned to the moisture room for additional days, depending on the curing duration and test scheme. The detailed test scheme of the studied UHPCs (both plain and fiber-reinforced) are presented in Table 4. The displacement at the mid-span of the beam was evaluated using an LVDT placed at the bottom center of the beam specimen. The flexural strength of the studied UHPCs was determined according to ASTM C1609 [48].

3. Experimental results on plain UHPCs (Phase I)

The results of compressive and splitting-tensile strengths, along with drying shrinkage for different V_A/V_{cm} as functions of curing durations are presented in Table 5. For the 28-day cured UHPCs, the compressive strength varied from 119 to 149 MPa, 118 to 151 MPa, and 108 to 139 MPa for V_A/V_{cm} of 0.80, 1.0, and 1.20, respectively. Similarly, the splitting-tensile strength ranged between 8.7 and 10.8 MPa, 8.6 to 10.5 MPa, and 8.1 to 10.3 MPa for the same V_A/V_{cm} . The average 120-day drying shrinkages were 0.1062, 0.0979, and 0.0896% for V_A/V_{cm} of 0.80, 1.0, and 1.20, respectively. The relative performance of binary, ternary, and quaternary UHPCs, as compared to that of the control (C100) UHPC, are illustrated in Fig. 7. The effects of cementitious materials compositions and V_A/V_{cm} on the bulk and dimensional stability properties of the studied plain UHPCs are discussed in the following subsections.

3.1. Effect of cementitious materials types and compositions

3.1.1. Compressive strength

The compressive strengths of the plain UHPCs, as a function of cementitious materials compositions and V_A/V_{cm} , are shown in Table 5 and Fig. 7. All UHPCs gained strength with the increase in testing duration due to their continued hydration. The UHPCs with binary fly ash combinations showed slower compressive strength development at early ages, as compared to the control UHPC (C100). However, due to increased pozzolanic reactivities, the 90-day cured binary UHPCs incorporating fly ash displayed similar or higher compressive strength when compared to the control UHPC. The binary UHPCs with natural pozzolans followed a similar trend as did fly ash in the binary UHPCs. The binary UHPCs containing GGBS followed the same trend as the control UHPC in

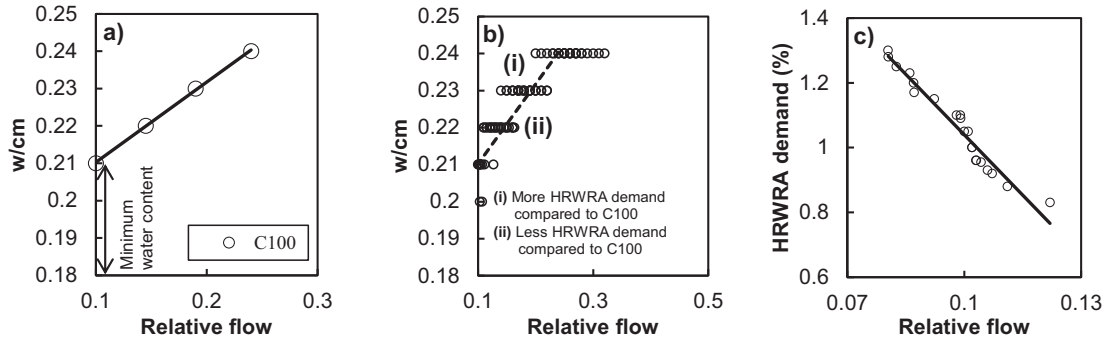


Fig. 3. Criteria for the selection of cementitious material combination: (a) minimum water content required for Type V cement (C100), (b) relative water demand at different w/cm, (c) demand of HRWRA based on relative flow.

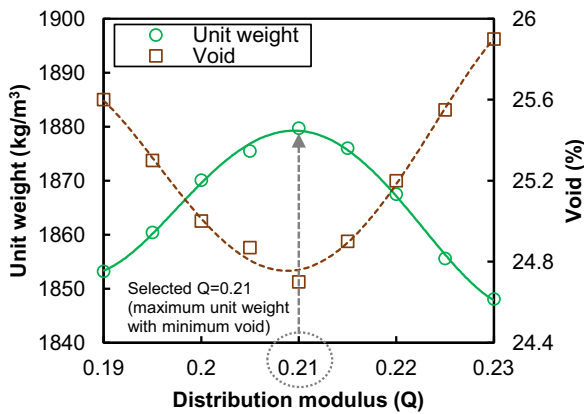


Fig. 4. Selection of distribution modulus based on unit weight of fine aggregate.

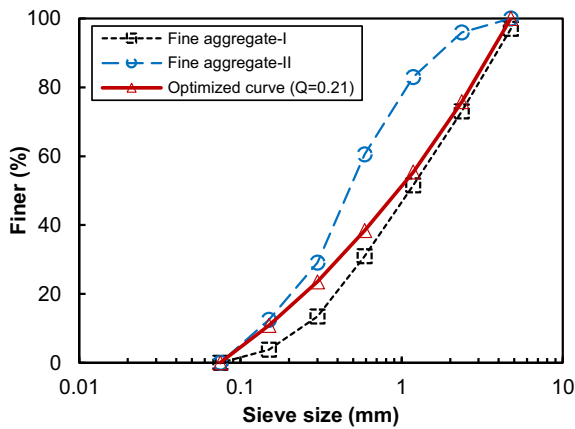


Fig. 5. Aggregate gradation of UHPCs, as per modified Andreasen and Andersen model.

compressive strength development over time. On the other hand, the UHPC with silica fume, as a partial replacement of Portland cement, surpassed the strength gains of the control UHPC at all curing ages. The presence of reactive fine silica helped the UHPCs to develop higher early strengths, as compared to the control UHPC. Irrespective of cementitious materials types and combinations, similar trends were observed for every V_A/V_{cm} .

Overall, the UHPCs containing fly ash or natural pozzolan displayed higher long-term compressive strengths, whereas UHPCs made with silica fume showed higher compressive strengths at early ages. In comparison to the control UHPC, GGBS containing UHPCs produced slightly lower compressive strengths at all cement replacement levels. Once calcium hydroxide (CH) was produced from the primary hydration reaction, the secondary pozzolanic reaction produced stronger calcium silicate hydrate (C-S-H), which was responsible for better later-age strength performance of the studied UHPCs having fly ash and natural pozzolans [50]. On the other hand, as shown in Fig. 2, silica fume had higher particle fineness than that of other cementitious materials which enabled it to produce superior early-age cementitious reactivities [51].

When 10% Portland cement was replaced by secondary cementitious materials, the UHPCs with 10% silica fume displayed the highest compressive strength, whereas the natural pozzolan showed the lowest results. At a 20% cement replacement level, UHPCs having GGBS showed higher compressive strength than UHPCs with fly ash and natural pozzolan. However, after 90 days of curing, the test samples incorporating fly ash showed the highest compressive strength amongst all binary mixtures with 20% cement replacement. When 30% of the Portland cement was replaced by secondary cementitious materials, the one and seven-day cured UHPCs' incorporating GGBS had higher compressive strengths. However, as the curing age increased, UHPCs with 30% fly ash and natural pozzolan showed higher compressive strengths, as compared to the UHPCs containing GGBS.

As mentioned earlier, an increase in fly ash/natural pozzolan content resulted in lower early strength development due to the pozzolanic materials' inactivity. With CH production, the secondary cementitious reaction of pozzolanic materials with CH resulted in better strength results for 90-day cured samples. However, the threshold for using these secondary cementitious materials depends on CH production in the matrix, as without it, these pozzolanic materials only act as filler materials in the UHPC matrix. Overall, in the binary blend UHPCs, mixtures with fly ash or silica fume performed better than slag and natural pozzolan. The spherical shape of the fly ash and silica fume enabled them to fill the micro voids within the matrix better than the irregular shaped GGBS or natural pozzolan (Fig. 1). As a result, slightly better strength performance can be seen with the binary UHPCs made with fly ash or silica fume, as compared to the UHPCs with same amount of natural pozzolan or GGBS.

Most of the mixtures having ternary blend displayed better compressive strength as compared to the control UHPC. Among all the ternary compositions, C80F15SF5, C80N15SF5,

Table 3
Mixture proportions of plain UHPCs.

Classification	Mixture ID ^a	V _A /V _{cm}	w/cm	kg/m ³								
				C ^b	F ^b	N ^b	S ^b	SF ^b	Agg ^b	HRWRA ^b	W ^b	
Control	C100	0.8	0.21	1280						910	12.0	262
	Binary	C90F10	0.8	0.21	1152	95				910	11.1	256
	C80F20	0.8	0.21	1024	189				910	10.9	249	
	C70F30	0.8	0.21	896	284				910	10.3	243	
	C60F40	0.8	0.21	768	379				910	10.2	236	
	C90N10	0.8	0.21	1152		84			910	11.2	254	
	C80N20	0.8	0.21	1024		149			910	11.2	241	
	C70N30	0.8	0.21	896		195			910	10.4	224	
	C90S10	0.8	0.21	1152			105		910	11.8	258	
	C80S20	0.8	0.21	1024			187		910	12.0	248	
	C70S30	0.8	0.21	896			245		910	12.3	233	
	C95SF5	0.8	0.21	1216				43	910	12.3	258	
	C90SF10	0.8	0.21	1152				82	910	12.4	252	
	C85SF15	0.8	0.21	1088				116	910	12.5	246	
Ternary	C80F15SF5	0.8	0.21	1024	142			36	910	11.3	247	
	C80N15SF5	0.8	0.21	1024		112		36	910	11.5	240	
	C80S15SF5	0.8	0.21	1024			140	36	910	12.1	246	
	C70F20SF10	0.8	0.21	896	189			63	910	12.1	235	
	C70N20SF10	0.8	0.21	896		130		63	910	12.1	222	
	C70S20SF10	0.8	0.21	896			163	63	910	12.3	229	
	C50F30SF20	0.8	0.21	768	284			109	910	12.6	237	
	C50N30SF20	0.8	0.21	768		167		109	910	12.7	213	
	C50S30SF20	0.8	0.21	768			210	109	910	13.0	221	
Quaternary	C60F15S15SF10	0.8	0.21	768	142		105	54	910	12.4	218	
	C60F10S20SF10	0.8	0.21	768	95		140	54	910	12.5	215	
	C50F20N20SF10	0.8	0.21	640	189	93		45	910	12.3	197	
Control	C100	1	0.21	1184					1052	12.0	243	
	Binary	C90F10	1	0.21	1065	88			1052	11.1	237	
	C80F20	1	0.21	947	175			1052	10.9	230		
	C70F30	1	0.21	828	263			1052	10.2	224		
	C60F40	1	0.21	710	350			1052	10.2	218		
	C90N10	1	0.21	1065		77		1052	11.1	235		
	C80N20	1	0.21	947		138		1052	11.1	222		
	C70N30	1	0.21	828		181		1052	10.3	207		
	C90S10	1	0.21	1065			97	1052	11.8	238		
	C80S20	1	0.21	947			173	1052	12.0	229		
	C70S30	1	0.21	828			226	1052	12.3	215		
	C95SF5	1	0.21	1124				40	1052	12.2	238	
	C90SF10	1	0.21	1065				75	1052	12.4	233	
	C85SF15	1	0.21	1006				107	1052	12.5	227	
Ternary	C80F15SF5	1	0.21	947	131			34	1052	11.3	228	
	C80N15SF5	1	0.21	947		103		34	1052	11.4	222	
	C80S15SF5	1	0.21	947			129	34	1052	12.1	227	
	C70F20SF10	1	0.21	828	175			59	1052	12.0	217	
	C70N20SF10	1	0.21	828		120		59	1052	12.1	206	
	C70S20SF10	1	0.21	828			151	59	1052	12.3	212	
	C50F30SF20	1	0.21	710	263			101	1052	12.5	219	
	C50N30SF20	1	0.21	710		155		101	1052	12.7	196	
	C50S30SF20	1	0.21	710			194	101	1052	12.9	204	
Quaternary	C60F15S15SF10	1	0.21	710	131		97	50	1052	12.4	201	
	C60F10S20SF10	1	0.21	710	88		129	50	1052	12.5	199	
	C50F20N20SF10	1	0.21	592	175	86		42	1052	12.2	182	
Control	C100	1.2	0.21	1101					1174	11.9	226	
	Binary	C90F10	1.2	0.21	991	81			1174	11.0	220	
	C80F20	1.2	0.21	881	163			1174	10.8	214		
	C70F30	1.2	0.21	771	244			1174	10.2	209		
	C60F40	1.2	0.21	660	326			1174	10.1	203		
	C90N10	1.2	0.21	991		72		1174	11.1	218		
	C80N20	1.2	0.21	881		128		1174	11.0	207		
	C70N30	1.2	0.21	771		168		1174	10.2	193		
	C90S10	1.2	0.21	991			90	1174	11.8	221		
	C80S20	1.2	0.21	881			160	1174	11.9	213		
	C70S30	1.2	0.21	771			211	1174	12.3	200		
	C95SF5	1.2	0.21	1046				37	1174	12.2	222	
	C90SF10	1.2	0.21	991				70	1174	12.4	217	
	C85SF15	1.2	0.21	936				99	1174	12.5	211	
Ternary	C80F15SF5	1.2	0.21	881	122			31	1174	11.3	212	
	C80N15SF5	1.2	0.21	881		96		31	1174	11.4	206	
	C80S15SF5	1.2	0.21	881			120	31	1174	12.0	211	
	C70F20SF10	1.2	0.21	771	163			55	1174	12.0	202	
	C70N20SF10	1.2	0.21	771		112		55	1174	12.0	191	
	C70S20SF10	1.2	0.21	771			140	55	1174	12.2	197	
	C50F30SF20	1.2	0.21	660	244			94	1174	12.5	204	

Table 3 (continued)

Classification	Mixture ID ^a	V _A /V _{cm}	w/cm	kg/m ³								
				C ^b	F ^b	N ^b	S ^b	SF ^b	Agg ^b	HRWRA ^b	W ^b	
Quaternary	C50N30SF20	1.2	0.21	660		144			94	1174	12.7	182
	C50S30SF20	1.2	0.21	660			181		94	1174	12.9	190
	C60F15S15SF10	1.2	0.21	660	122			90	47	1174	12.4	187
	C60F10S20SF10	1.2	0.21	660	81			120	47	1174	12.5	185
	C50F20N20SF10	1.2	0.21	550	163	80			39	1174	12.1	169

1 kg/m³ = 1.685 lb/yd³

^a Mixture ID: number after C, F, N, S, and SF indicates percentage of respective cementitious materials. For example, C90F10 means 90% cement and 10% class F fly ash.

^b C: Cement; ^bF: Class F fly ash; ^bN: Natural pozzolan; ^bS: Ground granulated blast-furnace slag; ^bSF: Silica fume; ^bAgg: Aggregate; ^bHRWRA: High-range water reducing admixture; ^bW: Water

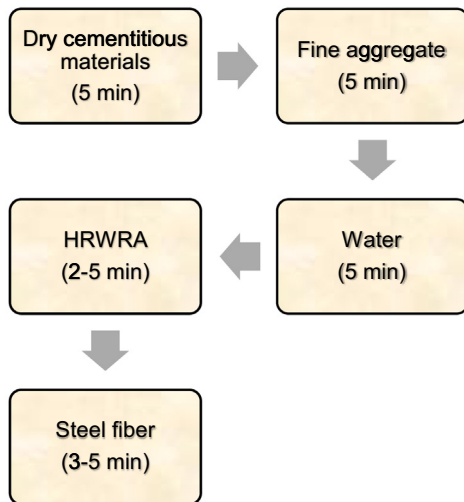


Fig. 6. UHPCs' mixing sequence.

C70F20SF10, and C70N20SF10 displayed excellent compressive strength, with a minimum 28-day strength of 120 MPa and 90-day compressive strength of 150-MPa. Early age pozzolanic reactivity of the silica fume facilitated the early strength development, while the secondary pozzolanic activity of fly ash/natural pozzolan helped in the long-term compressive strength gain of the studied UHPCs. UHPCs with more than 30% of Portland cement replaced by fly ash/GGBS/natural pozzolan did not achieve the target 28- and 90-day compressive strengths of 120 MPa or 150 MPa, respectively. The probable reason is that with conventional curing, UHPCs with a high amount of fly ash/GGBS/natural pozzolan did not react entirely. For this reason, several investigators have tried heat curing to maximize the pozzolanic material hydration [52,53].

Quaternary UHPCs incorporating a high amount of fly ash, GGBS, and natural pozzolan displayed lower compressive strengths at one and seven days curing durations. However, six out of nine mixtures achieved compressive strengths of 120 MPa and 150 MPa at 28- and 90-day curing. Perhaps, the amount of secondary cementitious materials in the quaternary mixtures exceeded the availability of CH to effectively activate these secondary cementitious materials [50].

When 20% of Portland cement replaced with 20% fly ash (Binary UHPC), compared with 15% fly ash and 5% silica fume having UHPC (Ternary UHPC), improvement was observed in the ternary UHPC. Similar improvements were also observed for ternary natural pozzolan and silica fume, as well as ternary GGBS and silica fume having UHPC, when compared to the binary UHPC with 20% natural pozzolan/GGBS as a partial replacement of Portland cement. At the 30% Portland cement replacement level, all ternary UHPCs displayed superior performance over binary UHPCs. Smaller particle size of silica fume contributed to the larger surface area which

Table 4
Test details of the studied UHPCs.

Phase I: Plain UHPCs			
Tests	Specimen details	Test age (days) ^b	Standards
Flow	Freshly mixed UHPCs	–	ASTM C230 [41]
Unit weight	Disk (100 mm diameter and 50 mm height)	1	ASTM C642 [44]
Compressive strength	Cylinder (50 mm diameter and 100 mm height)	1, 7, 28, and 90	ASTM C39 [45]
Splitting-tensile strength	Cylinder (50 mm diameter and 100 mm height)	28	ASTM C496 [46]
Drying shrinkage	Beam (25 × 25 × 250 mm)	120	ASTM C596 [47]
Phase II: Fiber-reinforced UHPCs ^a			
Flow	Freshly mixed UHPCs	–	ASTM C230 [41]
Unit weight	Disk (100 mm diameter and 50 mm height)	1	ASTM C642 [44]
Compressive strength	Cylinder (50 mm diameter and 100 mm height)	28	ASTM C39 [45]
Splitting-tensile strength	Cylinder (50 mm diameter and 100 mm height)	28	ASTM C496 [46]
Load-deflection response	Beam (50 × 50 × 200 mm)	28	ASTM C1609 [48]
Flexural strength	Beam (50 × 50 × 200 mm)	28	ASTM C1609 [48]
Flexural strain	Beam (50 × 50 × 200 mm)	28	ASTM C1609 [48]
Elastic modulus	Cylinder (75 mm diameter and 150 mm height)	28	ASTM C469 [49]
Drying shrinkage	Beam (25 × 25 × 250 mm)	120	ASTM C596 [47]

^a For comparison 11 plain UHPCs were also selected for these tests, ^b four specimen prepared per test age.

enabled silica fume to react at the early stages with free lime to produce C-S-H. In addition, the unreacted spherical silica fume had the ability to fill the smaller voids that other pozzolanic materials could not reach. For this reason, most of the ternary UHPCs displayed higher compressive strength as compared to that of the quaternary and binary UHPC blends. However, for quaternary blends, the presence of very high amounts of primarily unreactive pozzolans and a lack of CH produced from the binders to trigger the secondary reaction, as well as the size of the pozzolanic materials and availability of free water for secondary hydration, played important roles in the lower compressive strength gains, when compared to those of the binary/ternary UHPC blends. To support this statement, Yazici et al. [54] reported that, large number of cementitious particles remains unhydrated even after 28 days of curing due to lack of available water for hydration. Mehta and Monterio [55] mentioned that, pozzolanic material larger than 45 μm does not have the ability to participate in the secondary pozzolanic reaction to produce hydration product. As can be seen in Fig. 2, some of the fly ash/natural pozzolan/slag had particle size

Table 5
Compressive and splitting-tensile strength, along with drying shrinkage of UHPCs at different V_A/V_{cm} .

Classifications	Mixture ID	$V_A/V_{cm} = 0.8$						$V_A/V_{cm} = 1.0$						$V_A/V_{cm} = 1.2$						
		f_{c-1D}		f_{c-7D}		f_{c-28D}		f_{c-1D}		f_{c-7D}		f_{c-28D}		f_{c-1D}		f_{c-7D}		f_{c-28D}		
		(MPa)	(MPa)	(MPa)	(MPa)	(MPa)	(MPa)	(MPa)	(MPa)	(MPa)	(MPa)	(MPa)	(MPa)	(MPa)	(MPa)	(MPa)	(MPa)	(MPa)	(MPa)	
Control	C100	63	105	134	153	9.4	0.103	62	102	128	152	9.3	0.092	61	100	125	150	9.1	0.087	
Binary	C90F10	57	103	133	–	9.4	0.086	54	91	129	–	9.2	0.078	54	91	123	–	9.1	0.071	
	C80F20	53	94	128	158	9.6	0.084	51	89	128	154	9.2	0.076	52	84	122	151	9.0	0.068	
	C70F30	53	103	133	160	9.3	0.076	50	85	126	150	9.0	0.070	50	81	120	150	8.8	0.064	
	C60F40	49	95	124	157	9.2	0.072	46	74	119	147	8.6	0.066	46	74	113	150	8.1	0.061	
	C90N10	56	98	129	166	9.4	0.095	53	97	126	144	9.2	0.088	54	88	121	143	9.0	0.075	
	C80N20	54	97	127	151	9.3	0.086	54	89	123	145	8.9	0.078	52	84	119	146	8.9	0.071	
	C70N30	48	99	130	143	8.8	0.081	50	87	118	133	8.7	0.072	50	81	116	138	8.6	0.065	
	C90S10	59	93	125	167	8.8	0.110	65	103	127	149	8.9	0.098	61	96	123	148	8.9	0.087	
	C80S20	63	111	134	149	9.4	0.100	64	100	129	148	9.2	0.091	56	89	119	143	9.2	0.086	
	C70S30	64	111	134	152	8.9	0.096	68	104	127	148	8.9	0.084	57	91	119	139	8.8	0.080	
	C95SF5	73	118	140	165	9.8	0.116	71	114	140	171	9.5	0.106	65	109	131	168	9.4	0.096	
	C90SF10	74	120	149	168	10.5	0.120	74	124	147	175	10.0	0.110	71	117	138	164	9.8	0.101	
	C85SF15	75	120	149	–	10.8	0.130	75	126	151	177	10.5	0.116	72	119	139	–	10.3	0.103	
	Ternary	C80F15SF5	71	116	141	147	9.8	0.109	64	113	137	165	9.6	0.100	61	101	129	153	9.5	0.093
		C80N15SF5	70	115	139	150	9.6	0.110	60	107	134	158	9.5	0.102	59	96	127	151	9.3	0.094
C80S15SF5		69	102	128	139	9.5	0.116	67	115	132	159	9.5	0.106	64	104	124	149	9.5	0.096	
C70F20SF10		64	120	148	131	9.8	0.121	60	103	140	144	9.9	0.114	59	97	131	132	9.2	0.098	
C70N20SF10		59	112	144	136	9.7	0.122	57	105	136	151	9.8	0.112	59	99	130	145	9.1	0.100	
C70S20SF10		65	109	139	148	10.3	0.125	62	106	135	145	9.8	0.114	63	101	130	146	9.3	0.098	
C50F30SF20		53	97	126	138	9.4	0.127	52	84	126	145	9.2	0.111	45	75	116	128	8.7	0.101	
C50N30SF20		56	91	119	133	10.1	0.137	53	86	120	129	9.3	0.119	45	76	113	121	8.5	0.106	
C50S30SF20		57	99	127	149	9.3	0.140	54	91	122	134	8.7	0.122	50	83	117	125	8.3	0.108	
Quaternary		C60F15S15SF10	59	109	132	144	8.7	0.112	52	92	125	140	8.6	0.100	48	82	116	127	8.6	0.093
	C60F10S20SF10	60	102	131	151	9.2	0.097	47	88	127	145	9.2	0.113	46	80	112	131	9.2	0.118	
	C50F20N20SF10	54	72	123	154	9.2	0.090	45	70	118	148	9.2	0.107	40	72	108	137	9.1	0.109	

Note: 1 MPa = 145 Psi; f_{c-1D} , f_{c-7D} , f_{c-28D} , and f_{c-90D} denotes compressive strength at 1-day, 7-day, 28-day, and 90-day, respectively; f_{t-28D} denote splitting-tensile strength at 28-day; D_{120D} denote drying shrinkage at 120-day

larger than 45 μm which explains the lower strength development at higher pozzolan replacement for quaternary blends.

3.1.2. Splitting-Tensile strength

The splitting-tensile strengths of the plain UHPCs, as a function of cementitious materials compositions and V_A/V_{cm} are documented in Table 5 and Fig. 7. Nearly all splitting-tensile strengths of the binary, ternary, and quaternary UHPCs displayed similar trends to those of the compressive strength. However, for the studied plain UHPCs, a higher cementitious material content had less influence in improving tensile strength than it had on compressive strength. The average compressive-to-splitting-tensile strength ratios were 14, 13.95, and 13.6, for aggregate-to-cementitious material ratios of 0.80, 1.0, and 1.2, respectively, whereas for conventional concrete the ratio mostly varies between 8 and 12 [56]. A study on UHPCs conducted by Meng et al. [30] also found a very high compressive-to-splitting-tensile strength ratio of 16.8. It is possible that the absence of coarse aggregate changes the interfacial transition zone of the plain UHPCs in sustaining tensile force. This limitation is not well documented in the literature, as nearly all studied UHPCs contained some sort of fiber to compensate for the brittle failure of plain UHPCs. Therefore, it can be said that using plain UHPCs will not be sufficient for the requirement of all mechanical properties.

The average 28-day cured splitting-tensile strength of the fly ash incorporating binary UHPCs varied from 9.2 to 9.4 MPa, 8.6 to 9.2 MPa, and 8.1 to 9.1 MPa, for aggregate-to-cementitious materials ratios of 0.80, 1.0, and 1.2, respectively. The binary UHPCs with natural pozzolan/GGBS showed similar splitting-tensile strengths at the 28-day testing age. With an increase of the fly ash/natural pozzolan content from 10 to 30%, the split tensile strength decreased. In contrast to fly ash/natural pozzolan, increases in silica fume content in the binary UHPCs improved

the splitting tensile strength results. The binary UHPCs with silica fume displayed average 3, 9, and 14% increases in splitting-tensile strength, as compared to the control UHPCs at 5, 10, and 15% replacement levels. When fly ash was substituted for portions of Portland cement at 10 and 20% by weight, nearly no decrease in splitting tensile strength was observed. However, with 30 and 40% fly ash, on average 3 and 7% lower splitting tensile strengths were observed as compared to that of the control UHPC. Amongst all the studied UHPCs, C85SF15 displayed the highest splitting-tensile strength for all aggregate-to-cementitious material ratios, whereas, C60F15S15SF10 and C60F40 displayed the lowest average splitting-tensile strength values as compared to that of the control UHPC.

Overall, in the binary blend UHPCs, the increase of natural pozzolan/fly ash/ slag resulted in decreased splitting-tensile strength when compared to that of the control UHPC, whereas, increased silica fume content improved the splitting-tensile strength of the binary silica blended UHPCs. This phenomenon can be explained by the highly reactive silica triggering early hydration and fly ash/slag/natural pozzolan's inability to be reactive during early hydration ages. This is also in-line with the compressive strength performance, as at 28 days, the compressive strength of UHPCs incorporating fly ash/natural pozzolan were lower than the control UHPC. However, 90-day binary UHPCs with cured fly ash surpassed the control UHPC. The splitting-tensile strength of ternary and quaternary blend UHPCs followed a similar pattern as compressive strength discussed in the previous section.

3.1.3. Drying shrinkage

Table 5 and Fig. 7 document the 120-day drying shrinkage results of the 78 studied UHPCs. Secondary cementitious materials had significant effects on the concretes' drying shrinkage, with fly ash performing the best and silica fume performing the worst

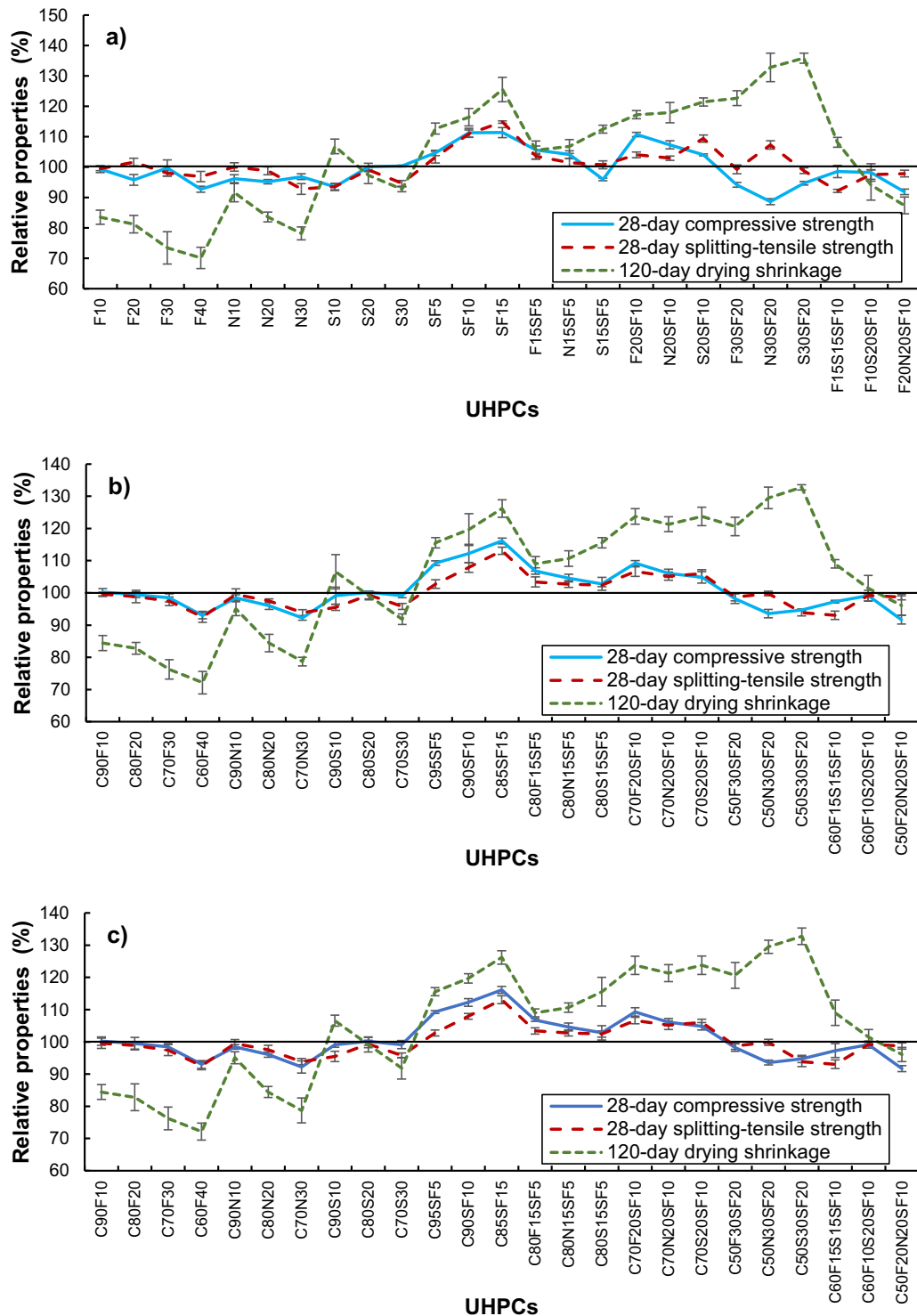


Fig. 7. Relative properties of the UHPCs, as compared to the control UHPC (C100) (a) for an aggregate-to-cementitious materials ratio of 0.8, (b) for an aggregate-to-cementitious materials ratio of 1.0, (c) for an aggregate-to-cementitious materials ratio of 1.2.

against drying shrinkage. UHPCs made with GGBS displayed similar shrinkage performance as the control mixture. The presence of unhydrated cementitious particles having fly ash/natural pozzolan minimized drying shrinkage by filling the voids, which provided additional dimensional stability to the UHPCs. On the other hand, extra fine silica fume consumed more water for hydration and resulted in higher drying shrinkage. Karim et al. [13] also con-

cluded that higher silica fume amounts resulted in higher drying shrinkage.

All ternary blend UHPCs displayed higher drying shrinkage as compared to the control UHPC, and mixtures with silica fume triggered UHPC drying shrinkage increases. However, UHPCs with 5% silica fume and 15% fly ash/natural pozzolan displayed only 6.5% higher drying shrinkage in comparison to that of the control UHPC.

UHPC blends having 20% silica fume displayed highest drying shrinkage amongst all mixtures. However, ternary and quaternary blend UHPCs made using both silica fume and natural pozzolan and/or fly ash displayed better performance against drying shrinkage compared to those of the binary UHPCs with silica fumes. Quaternary blend UHPCs with 20% fly ash and 20% natural pozzolan and 10% silica fume showed lower drying shrinkage as compared the control UHPC. The presence of fly ash and natural pozzolan compensated for the higher drying shrinkage exhibited by the silica fume, as seen in the binary blend UHPCs made with silica fume [57].

3.2. Effect of V_A/V_{cm} on compressive and Splitting-Tensile Strengths, and drying shrinkage

Table 5 and Fig. 8a present the effect of V_A/V_{cm} on the average compressive strength of the plain UHPCs at various curing durations. With the increase in curing age, the compressive strength also increased. On average, the UHPCs with $V_A/V_{cm} = 0.80$ attained 46 and 78% of their 28-day compressive strength at one and seven days, respectively. Similar compressive strength developments were found for $V_A/V_{cm} = 1.0$ and 1.20. On average, the 90-day compressive strengths were 13, 17, and 18% higher than the 28-day compressive strength for the UHPCs having $V_A/V_{cm} = 0.80, 1.0,$ and 1.2, respectively. For $V_A/V_{cm} = 0.80$ and 1.0, fifteen out of the twenty-six UHPCs achieved the minimum compressive strengths of 120 and 150 MPa, respectively, at 28 and 90 days curing durations. When the $V_A/V_{cm} = 1.2$ was used, 12 out of 26 UHPCs produced the minimum compressive strength of 120 and 150 MPa for the same curing ages.

Generally, with the increase of V_A/V_{cm} from 0.80 to 1.2, the compressive strength decreased. However, the effects were minimal at later curing durations. For example, at the 7-day testing an average of 6 and 12% reduction in compressive strength was observed for UHPCs having $V_A/V_{cm} = 1.0$ and 1.2, respectively, whereas for 90-day testing, the reduction in compressive strengths were 3 and 7% when compared to those of the UHPC with $V_A/V_{cm} = 0.80$. Overall, while cementitious materials content can make a sizeable impact on strength, the proportions of aggregate-to-cementitious materials also plays a role on strength, due to contributions of quality and amount of aggregate on the resulting w/cm, porosity, and interfacial zone.

The effect of V_A/V_{cm} on the average 28-day splitting-tensile strength of the plan UHPCs is shown in Fig. 8b and Table 5. Similar to the results of strength in compression, with the increase of V_A/V_{cm} , a decrease in the splitting-tensile strength was observed. On

average, 9.5, 9.3, and 9.0 MPa splitting-tensile strengths were obtained for the studied UHPCs using $V_A/V_{cm} = 0.80, 1.0,$ and 1.20, respectively. Also, on average, 2.4 and 4.8% reductions in splitting-tensile strengths were observed for $V_A/V_{cm} = 1.0$ and 1.2, respectively, as compared to $V_A/V_{cm} = 0.80$. Higher cementitious material amounts resulted in slightly higher tensile strength values; however, the differences were not significant. As previously discussed, significantly high 28-day compressive strength-to-splitting-tensile strength ratio was observed for the studied UHPCs; however, as the V_A/V_{cm} increased, this strength ratio decreased, indicating the higher fine aggregate amounts improved splitting-tensile strength more than the compressive strength. Therefore, the use of very high cementitious material amounts does not improve compressive strength more than splitting-tensile strength. For this reason, in nearly all studies conducted on UHPCs, researchers included some sort of fibers to improve tensile strength performance.

The effect of V_A/V_{cm} on the average 120-day drying shrinkage of the plain UHPCs is shown in Fig. 8c and Table 5. In general, with the increase of V_A/V_{cm} , a decrease in drying shrinkage was observed. On average, 0.106, 0.097, and 0.087% drying shrinkage was obtained using V_A/V_{cm} of 0.80, 1.0, and 1.20, respectively. Moreover, on average, a 9.1 and 17.7% reduction in drying shrinkage were observed for V_A/V_{cm} of 1.0 and 1.2, respectively, as compared to that of the V_A/V_{cm} of 0.80. This can be attributed to the lower cementitious materials content and higher restraining effect of the filler materials as the V_A/V_{cm} of the UHPCs increased.

3.3. Optimized plain UHPCs

In the first phase of the study, three aggregate-to-cementitious materials ratios (0.80, 1.0, and 1.20) were used to assess the bulk properties and dimensional stability of the studied UHPCs. The average 28-day compressive strength test shows that UHPCs with the V_A/V_{cm} equals to 1.20 displayed 7% lower compressive strength and 5% lower splitting-tensile strength than that of the V_A/V_{cm} of 0.80. Interestingly, as the curing duration increased from 28-day to 90-day, the average compressive strength of UHPCs made using V_A/V_{cm} of 1.20 was only 3% lower than the V_A/V_{cm} of 0.80. In contrast, the average 120-day drying shrinkage of UHPCs having V_A/V_{cm} of 0.80 was significantly (22%) higher than that of the UHPCs made using V_A/V_{cm} of 1.20. Considering these outcomes, V_A/V_{cm} of 1.20 was selected for the Phase II of this study.

Amongst the 26 cementitious material compositions used in the first phase of this study, four binary (out of 13), four ternary (out of nine), and two quaternary (out of three) cementitious composi-

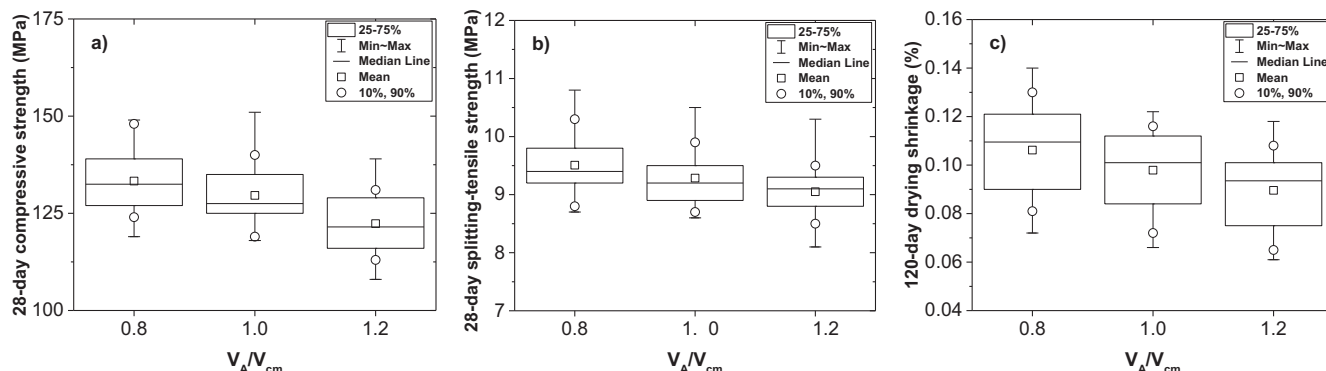


Fig. 8. Effects of aggregate-to-cementitious materials ratios on UHPCs' (a) 28-day compressive strength, (b) 28-day splitting-tensile strength, and (c) 120-day drying shrinkage.

tions were selected based on their mechanical and dimensional stability performance within their own respective groups. Additionally, concrete cost was considered when similar properties were obtained in the same cement blend group. The price distribution of Portland cement and slag is similar, and it seemed that addition of GGBS did not add much benefit to the bulk and dimensional stability of the UHPCs incorporating GGBS. On the other hand, class F fly ash and natural pozzolan significantly improved the long-term strength properties, as well as the 120-day drying shrinkage behavior. For this reason, in the Phase II, GGBS was only incorporated in one fiber-reinforced UHPC. Silica fume addition improved bulk properties significantly, however, it negatively impacted dimensional stability. Silica fume with fly ash/natural pozzolan provided both higher bulk properties and lower dimensional stability. For these reasons, the ternary UHPCs selected for Phase II study contained silica fume combined with fly ash or natural pozzolan.

4. Fiber-Reinforced UHPCs (Phase II)

Based on the results of the strength properties and drying shrinkage of the UHPCs studied in Phase I, a total of 40 UHPCs (11 plain UHPCs and 29 steel fiber-reinforced UHPCs) with 11 binder combinations were selected to study the performance of fiber-reinforced UHPCs. The Phase II mixture proportions for fiber-reinforced UHPCs are presented in Table 6. Their batching procedure was the same as the one presented in Section 2.5. The investigated properties included compressive strength, splitting-tensile resistance, flexural strength, load–deflection response, flexural strain, elastic modulus, and drying shrinkage. The details of all the tests performed in this phase are given in Table 4.

5. Experimental results on Fiber-Reinforced UHPC (Phase II)

Table 7 summarizes the bulk, shrinkage, and flexural strain properties of fiber-reinforced UHPCs and UHPCs without steel fibers. A detailed discussion is provided in the following subsections.

5.1. Flow and unit weight

The UHPCs' flow diameters and demolded unit weights are presented in Table 7. A satisfactory flow spread diameter of 250 ± 25 mm was attained for all UHPCs. UHPCs containing steel fibers required additional HRWRA to maintain the required flow spread diameter. Fly ash's spherical shape (Fig. 1) gave the mixtures additional flowability and a lower demand for HRWRA. On the other hand, UHPCs containing silica fume, with a very high surface areas, (Fig. 2) required a higher amount of HRWRA. On average, 2402, 2490, and 2546 kg/m³ unit weight was obtained using 0, 2, and 3% steel fibers, respectively. A typical unit weight of UHPCs varies from 2300 to 2700 kg/m³ [20]. Due to the high relative density of the steel fibers, the UHPCs containing 2 and 3% steel fibers showed higher unit weights as compared to those of the companion plain UHPCs.

5.2. Effect of steel fiber content and shape

5.2.1. Compressive strength

The 28-day compressive strength of the UHPCs containing 2 and 3% hooked and straight steel fibers is documented in Table 7 and Fig. 9a. In general, the introduction of fibers improved the UHPCs' compressive strength to some extent, and UHPCs made with 3% steel fibers produced slightly higher compressive strengths than those UHPCs incorporating 2% steel fibers. When 2% hooked steel

fiber was added, the average compressive strength improved by 3% as compared to the control UHPC without steel fibers. With the introduction of 3% hooked fiber, the corresponding gain in average compressive strength was 6%. The increases in the compressive strength, with increases in fiber content, can be attributed to the anticipated increase in the matrix stiffness of the fiber-containing UHPCs; however, these improvements were minimal. Several other studies also reported similar finding [58,59]. The addition of 2 and 3% straight steel fibers to the UHPCs resulted in an average increase of 2% in compressive strength as compared to those of the UHPCs made with the hooked fibers, possibly due to better interfacial bonding between the matrix and straight fibers.

5.2.2. Splitting-Tensile strength

The 28-day splitting-tensile resistance of the UHPCs with 2 and 3% hooked and straight steel fibers is presented in Table 7 and Fig. 9b. The introduction of fibers significantly improved splitting-tensile strength. The UHPCs made with 3% steel fibers produced a significantly higher splitting-tensile strength as compared to the UHPCs made with 2% steel fibers. When 2% hooked steel fiber was added, the average splitting-tensile strength improved by 17% as compared to that of the plain UHPC. With the introduction of 3% hooked fiber, the corresponding gain in the average splitting-tensile strength was nearly 37%. Additionally, the test specimens having 2 and 3% straight fibers increased their average splitting-tensile resistance by 18 and 38%, respectively. This finding can be attributed to the anticipated increase in the matrix stiffness of the fiber-reinforced UHPCs. Additionally, steel fibers distributed localized stress to the surrounding concrete and acted as a crack arrester. The addition of 2 and 3% straight steel fibers resulted in a similar increase in splitting-tensile strength, as compared to those of the UHPCs made with the hooked fibers.

5.2.3. Load-Deflection Response, flexural Strength, and flexural strain

The mid-span load–deflection ($P-\delta$) response of the 28-day cured UHPC beams for both plain and fiber-reinforced UHPCs was determined and the representatives are depicted in Fig. 10. Fig. 10a shows the load–deflection response of the control UHPCs incorporating 0, 2 and 3% hooked steel fibers. The $P-\delta$ responses of all three UHPCs were linear until the deflection values reached near to 0.1 mm, at which plain UHPC reached its peak load and failed in a brittle manner. An increased load capacity was obtained when the fiber volume increased from 2% to 3%. The fiber-reinforced UHPCs showed a strain hardening response between 0.1 and 0.45 mm deflection for 2% fiber-reinforced UHPCs, and 0.1 to 0.80 mm deflection for 3% fiber-reinforced UHPC specimens. As the fiber content increased from 2 to 3%, the post-peak load retention capacity also increased. A similar trend was found for the UHPCs containing straight steel fibers as depicted in Fig. 10b. The failure sequence of fiber-reinforced UHPCs having 3% steel fibers is illustrated in Fig. 11. The steel fibers acted as a bridge to restrain crack development, and a clear demonstration of the strain-hardening and softening effect is depicted. Arora et al. [24] also documented a similar strain-hardening trend in the $P-\delta$ responses of fiber-reinforced UHPCs.

The 28-day flexural strength of the studied UHPCs are given in Table 7. Overall, significant improvement in flexural strength was observed when steel fibers were incorporated, with the addition of 2 and 3% hooked steel fibers resulting in average increases of 23 and 36%, respectively, when compared to those of the plain UHPCs. In comparison, improvements in the flexural strength of the UHPCs made with 2 and 3% straight steel fibers were 29 and 43%, respectively. The effects of fiber content and shape on the UHPCs' flexural strength is presented in Fig. 12. From the box-whisker plot, the shape of fiber had only a minor influence on flex-

Table 6
Mixture proportions of fiber-reinforced UHPCs.

Mixture ID ^a	V _A /V _{cm}	w/cm	C ^b	F ^b	N ^b	S ^b	SF ^b	Agg ^b	HRWRA ^b	W ^b	Fiber ^b
			kg/m ³								
C100-2%H	1.2	0.21	1101					1174	13.1	224	156
C95SF5-2%H	1.2	0.21	1046				37	1174	13.4	220	156
C90SF10-2%H	1.2	0.21	991				70	1174	13.6	216	156
C80F20-2%H	1.2	0.21	881	163				1174	11.9	213	156
C70F30-2%H	1.2	0.21	771	244				1174	11.2	208	156
C80F15SF5-2%H	1.2	0.21	881	122			31	1174	12.4	211	156
C80N15SF5-2%H	1.2	0.21	881		96		31	1174	12.5	205	156
C70F20SF10-2%H	1.2	0.21	771	163			55	1174	13.2	201	156
C70N20SF10-2%H	1.2	0.21	771		112		55	1174	13.2	190	156
C60F10S20SF10-2%H	1.2	0.21	660	81		120	47	1174	13.7	184	156
C50F20N20SF10-2%H	1.2	0.21	550	163	80		39	1174	13.3	168	156
C100-2%S	1.2	0.21	1101					1174	13.1	224	156
C95SF5-2%S	1.2	0.21	1046				37	1174	13.4	220	156
C80F20-2%S	1.2	0.21	881	163				1174	11.9	213	156
C70F30-2%S	1.2	0.21	771	244				1174	11.2	208	156
C80F15SF5-2%S	1.2	0.21	881	122			31	1174	12.4	211	156
C80N15SF5-2%S	1.2	0.21	881		96		31	1174	12.5	205	156
C100-3%H	1.2	0.21	1101					1174	14.9	222	234
C95SF5-3%H	1.2	0.21	1046				37	1174	13.2	220	234
C80F20-3%H	1.2	0.21	881	163				1174	12.4	214	234
C70F30-3%H	1.2	0.21	771	244				1174	13.7	208	234
C80F15SF5-3%H	1.2	0.21	881	122			31	1174	13.9	210	234
C80N15SF5-3%H	1.2	0.21	881		96		31	1174	16.5	202	234
C100-3%S	1.2	0.21	1101					1174	14.7	223	234
C95SF5-3%S	1.2	0.21	1046				37	1174	13.8	218	234
C80F20-3%S	1.2	0.21	881	163				1174	15.2	209	234
C70F30-3%S	1.2	0.21	771	244				1174	15.4	205	234
C80F15SF5-3%S	1.2	0.21	881	122			31	1174	18.3	205	234
C80N15SF5-3%S	1.2	0.21	881		96		31	1174	16.3	204	234

1 kg/m³ = 1.685 lb/yard³

^a Mixture ID: number after C, F, N, S, and SF indicates percentage of respective cementitious materials. 2%S, 2%H, 3%S, and 3%H after hyphen (-) denotes percentage of steel fiber used. For example, C95SF5-2%H means 95% cement and 5% silica fume and 2% hooked steel fiber.

^b C: Cement; ^bF: Class F fly ash; ^bN: Natural pozzolan; ^bS: Ground granulated blast-furnace slag; ^bSF: Silica fume; ^bAgg: Aggregate; ^bHRWRA: High-range water reducing admixture; ^bW: Water; ^bFiber: Steel fiber.

ural strength of the UHPCs. Mixtures incorporating 2% and 3% straight fibers showed 7 and 11% higher flexural strength, respectively, when compared with those made with hooked fibers. The addition of steel fibers had more influence on the UHPCs' flexural strength resistance than it did on their compressive strength.

The 28-day flexural strain evaluated from the load–deflection responses of the UHPCs are tabulated in Table 7. Due to the brittle nature of plain UHPCs, these mixtures had a very low flexural strain at peak load. As shown in Fig. 13, presence of steel fibers improved the flexural strain by arresting crack growth and generating strain-hardening before the peak strength was reached. The improvement in flexural strain capacity, due to the contribution of steel fibers, corroborates the increased ductility of the studied fiber-reinforced UHPCs.

5.2.4. Elastic modulus

Table 7 documents the 28-day elastic moduli of the studied UHPCs. Similar to the results of compressive strength, the addition of steel fibers did not have significant effects on the elastic moduli of the studied UHPCs. Yoo et al. [33] also reported minor improvement of elastic moduli in fiber-reinforced UHPCs. Inclusion of 2 and 3% hooked steel fibers resulted in average increases of 3 and 6%, respectively. In comparison, improvements in the elastic moduli of the UHPCs made with 2 and 3% straight steel fibers were 4 and 8%, respectively. Fig. 14 documents the effects of fiber contents and shapes on the elastic moduli of the studied UHPCs. The UHPCs made with straight steel fibers performed slightly better than the hooked steel fibers. Mixtures containing 2% and 3% straight fibers showed 7 and 11% higher elastic modulus, respectively, when compared to the companion UHPCs containing hooked fibers.

5.2.5. Drying shrinkage

The drying shrinkage of the plain and fiber-reinforced UHPCs is documented in Table 7. The effects of the cementitious materials and fine aggregate-to-cementitious materials ratio on the UHPCs' drying shrinkage were discussed in Section 3.1.3 and 3.2. The effect of steel fiber content and shape on the drying shrinkage as a function of time is shown in Fig. 15. Inclusion of steel fibers greatly restrained the drying shrinkage. Overall, the drying shrinkage of both plain and fiber-reinforced UHPCs peaked at about 60 days with minor increases thereafter. Straight steel fibers performed slightly better in restraining drying shrinkage due to better fiber to paste surface bonding. This finding is in line with the other mechanical properties, such as flexural strength and elastic modulus. On average, inclusion of 2 and 3% steel fiber resulted in 14 and 26% reductions of drying shrinkage as compared to that of the plain UHPCs. As can be seen, 3% steel fibers were more effective in reducing drying shrinkage than 2% steel fibers. Yoo et al. [33] also found 3% steel fiber to be optimum in reducing drying shrinkage.

6. Relationships between UHPCs' bulk properties

Various correlations were developed amongst compressive strength (120–150 MPa), splitting-tensile resistance, flexural strength, and elastic modulus of the studied plain and fiber-reinforced UHPCs. A suitable relationship, at a 95% confidence level, between 28-day cured compressive strength and splitting-tensile resistance is shown in Fig. 16. Increases in the UHPCs' compressive strength led to increased splitting-tensile strength for the studied UHPCs. The steel fiber content had more influence on splitting-tensile strength than it had on compressive strength.

Table 7
Summary of test results of Phase II study.

Mixture ID	Flow (mm)	γ_{con} (kg/m ³)	f'_{c-28D} (MPa)	f_{t-28D} (MPa)	f_{r-28D} (MPa)	E_{c-28D} (GPa)	D_{120D} (%)	ϵ_f (%)
C100	248	2470	125	9.1	11.8	38.9	0.087	0.00005
C95SF5	273	2451	131	9.4	13.2	41.8	0.096	0.00005
C90SF10	268	2432	138	9.8	14.3	44.0	0.101	0.00006
C80F20	270	2405	122	9.0	12.5	37.9	0.068	0.00004
C70F30	250	2374	120	8.8	12.2	37.2	0.064	0.00004
C80F15SF5	253	2388	129	9.5	13.3	42.2	0.093	0.00005
C80N15SF5	236	2386	127	9.3	12.7	41.2	0.094	0.00005
C70F20SF10	274	2372	131	9.2	12.7	41.5	0.098	0.00005
C70N20SF10	267	2369	130	9.1	11.9	39.9	0.100	0.00004
C60F10S20SF10	244	2385	123	9.2	12.7	37.4	0.086	0.00004
C50F20N20SF10	272	2393	120	9.1	10.7	35.3	0.083	0.00004
C100-2%H	241	2536	127	10.5	16.2	39.4	0.079	0.00102
C95SF5-2%H	247	2512	135	11.1	18.0	42.3	0.083	0.00107
C90SF10-2%H	244	2506	143	11.4	18.3	44.7	0.093	0.00119
C80F20-2%H	271	2475	125	10.6	15.4	39.2	0.059	0.00093
C70F30-2%H	269	2440	127	10.4	15.1	39.8	0.056	0.00078
C80F15SF5-2%H	248	2483	136	11.2	16.6	42.5	0.081	0.00165
C80N15SF5-2%H	250	2478	131	10.9	16.9	41.7	0.082	0.00144
C70F20SF10-2%H	248	2504	136	10.7	17.0	42.3	0.086	0.00190
C70N20SF10-2%H	251	2473	135	10.6	16.8	42.1	0.092	0.00187
C60F10S20SF10-2%H	245	2488	131	10.3	15.1	38.1	0.082	0.00111
C50F20N20SF10-2%H	242	2483	123	10.1	14.9	36.7	0.081	0.00099
C100-2%S	256	2531	127	10.6	16.8	39.9	0.078	0.00128
C95SF5-2%S	240	2506	134	11.0	18.5	42.4	0.083	0.00205
C80F20-2%S	247	2491	125	10.7	17.7	39.0	0.059	0.00085
C70F30-2%S	270	2446	128	10.6	17.3	40.1	0.056	0.00107
C80F15SF5-2%S	264	2490	135	11.1	18.7	43.7	0.078	0.00189
C80N15SF5-2%S	245	2481	133	11.0	17.3	42.6	0.080	0.00157
C100-3%H	251	2585	130	12.3	18.7	41.4	0.069	0.00385
C95SF5-3%H	255	2551	139	12.8	22.0	43.1	0.073	0.00449
C80F20-3%H	240	2540	127	12.2	17.5	39.8	0.054	0.00383
C70F30-3%H	246	2498	131	12.1	17.2	43.3	0.052	0.00352
C80F15SF5-3%H	265	2535	140	13.1	22.2	43.9	0.072	0.00532
C80N15SF5-3%H	261	2533	137	12.9	19.9	43.1	0.074	0.00443
C100-3%S	271	2592	131	12.5	20.7	41.9	0.067	0.00403
C95SF5-3%S	250	2583	141	13.0	23.1	44.7	0.074	0.00540
C80F20-3%S	255	2543	128	12.4	20.7	40.4	0.054	0.00448
C70F30-3%S	238	2506	133	12.3	19.7	42.8	0.053	0.00424
C80F15SF5-3%S	243	2535	143	13.1	24.7	45.0	0.068	0.00557
C80N15SF5-3%S	264	2545	137	13.0	23.0	43.9	0.070	0.00509

Note: 1 MPa = 145 Psi; γ_{con} denote unit weight; f'_{c-28D} denotes compressive strength at 28-day; f_{t-28D} denote splitting-tensile strength at 28-day; f_{r-28D} denote flexural strength at 28-day; E_{c-28D} denote elastic modulus at 28-day; D_{120D} denote drying shrinkage at 120-day; ϵ_f denote flexural strain at peak load.

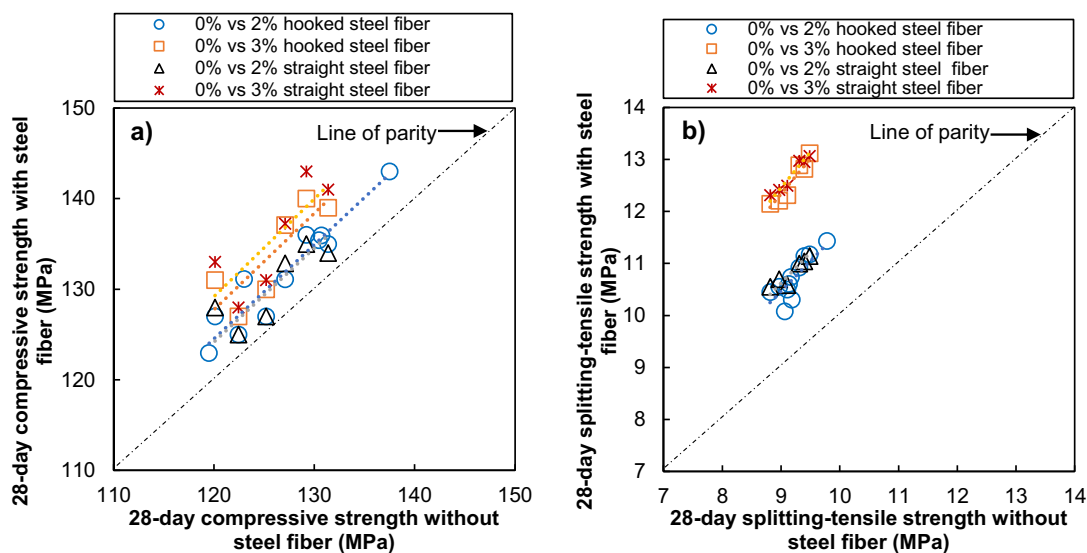


Fig. 9. Effect of steel fiber content and shape on UHPCs' (a) 28-day compressive strength, (b) 28-day splitting-tensile strength.

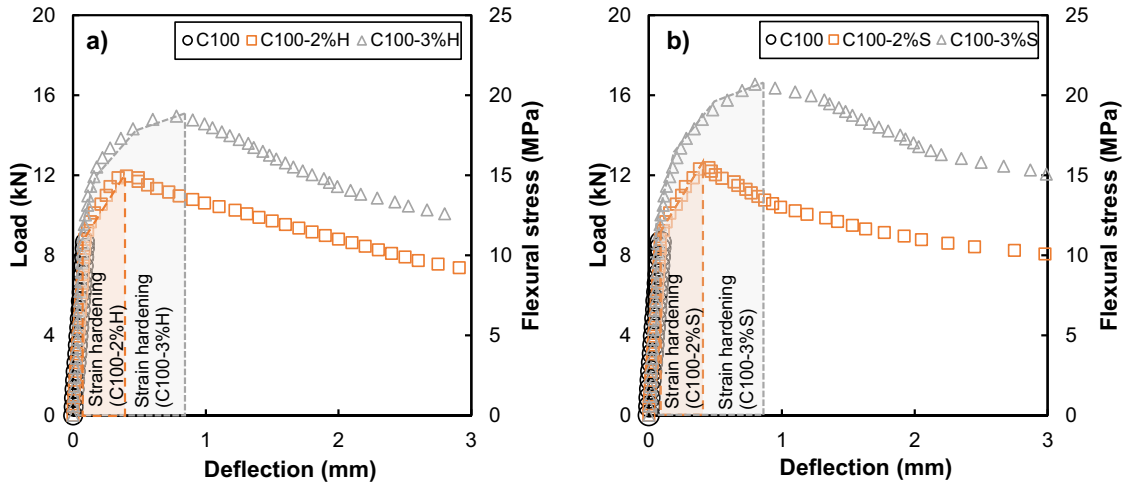


Fig. 10. Load-deflection response of plain and fiber-reinforced UHPCs: (a) with hooked steel fibers, (b) with straight steel fibers.

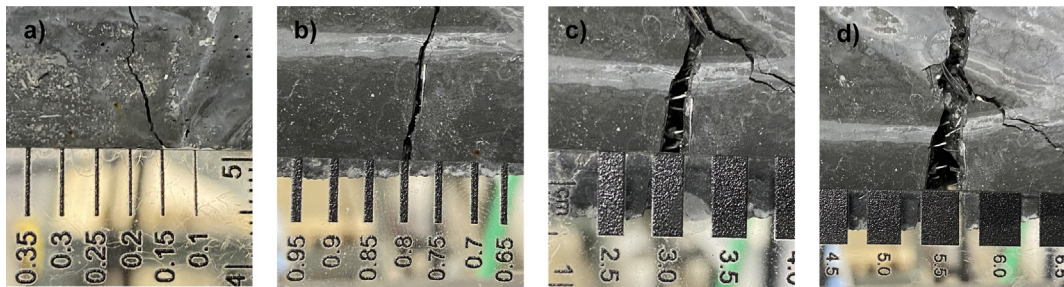


Fig. 11. Failure sequence of typical fiber-reinforced UHPC (C100-S3%), (a) first crack, (b) strain hardening, (c) softening, (d) failure of sample.

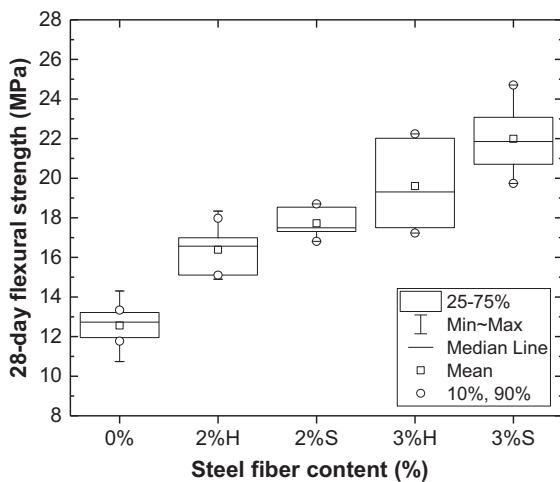


Fig. 12. Effects of steel fiber content and shape on UHPCs' 28-day flexural strength.

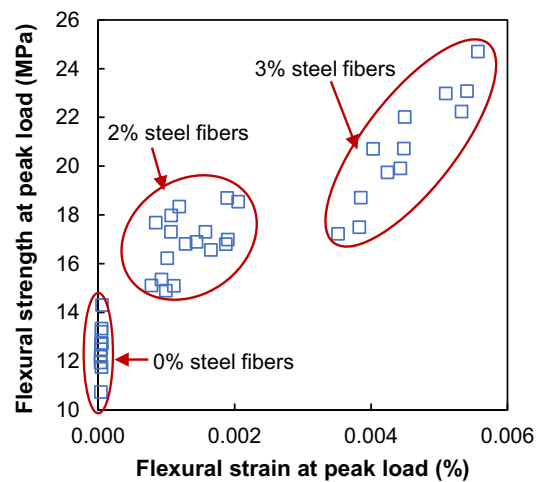


Fig. 13. Correlation between flexural strength and flexural strain at peak load.

Increases in steel fiber content also resulted in the reduced compressive-splitting-tensile strength ratios of the studied UHPCs. The relationship between the flexural and splitting-tensile strength of fiber-reinforced UHPCs, with a coefficient of determination (R^2) value of 0.92, is presented in Fig. 17. The proposed equation can be used to predict the splitting-tensile strength of UHPCs using flexu-

ral strength data. Compressive strength and modulus of elasticity relationships are well established in various codes and standards for conventional and high-strength concrete. An attempt was made to develop a correlation between compressive strength and modulus of elasticity of the studied UHPCs. Fig. 18 documents the most suitable relationship between compressive strengths and elastic

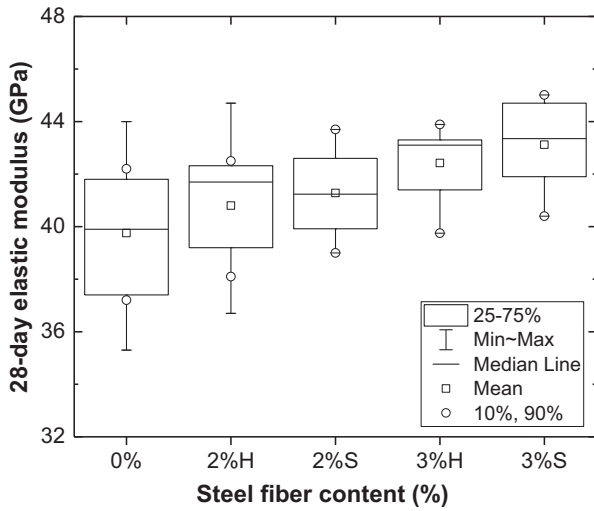


Fig. 14. Effect of steel fiber content and shape on 28-day elastic modulus of UHPCs.

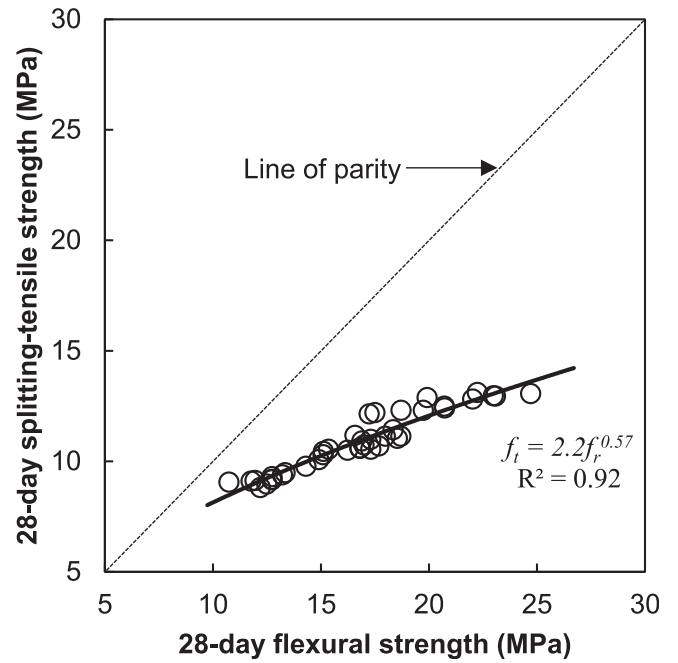


Fig. 17. Correlation between 28-day splitting-tensile and flexural strengths.

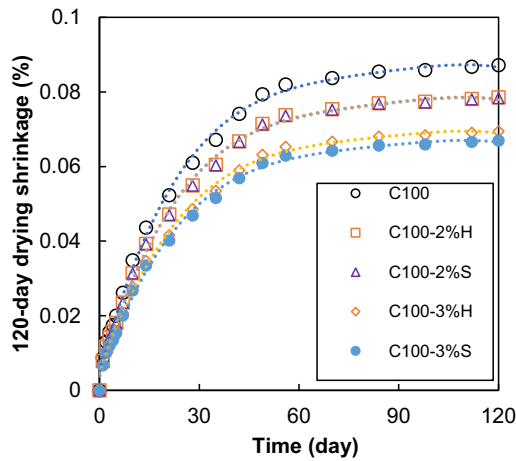


Fig. 15. Effects of steel fiber content and shape on UHPCs' drying shrinkage.

moduli, having a coefficient of determination (R^2) value 0.84. The

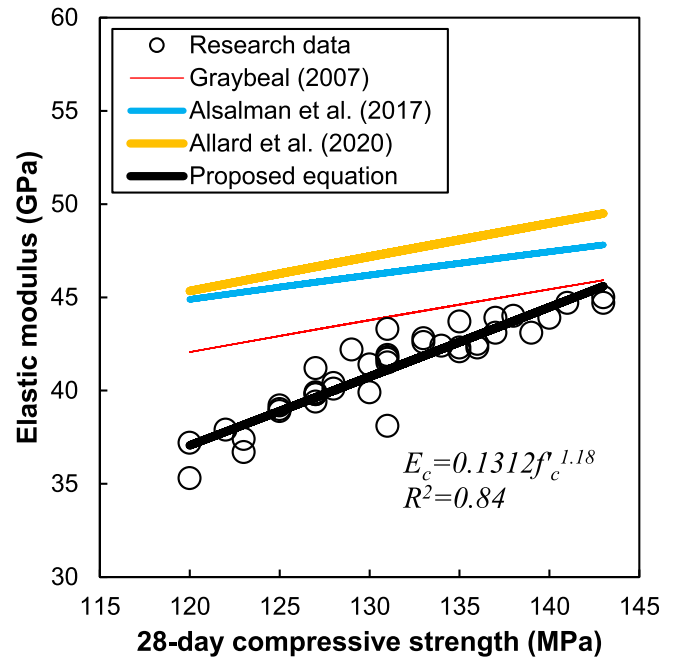


Fig. 18. Correlation between 28-day compressive strength and elastic modulus.

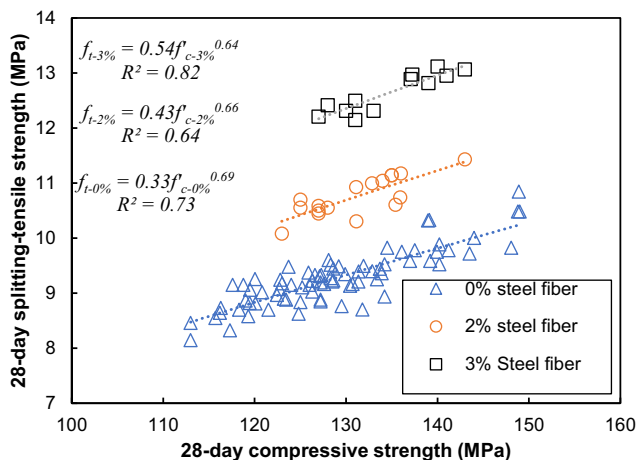


Fig. 16. Correlation between 28-day compressive and splitting-tensile strengths.

use of high amounts of cementitious materials and omission of coarse aggregate in UHPCs resulted in the relationship between compressive strength and elastic modulus that differed from that of the conventional UHPC concretes. A similar observation was also reported by Alsalman et al. [26].

7. Conclusions

Based on the results of this study, the following conclusions can be drawn:

- (1) The binary blend UHPCs containing fly ash or silica fume displayed higher strength properties than slag and natural pozzolan. Overall, amongst the studied binary, ternary, and quaternary cement blend UHPCs; ternary blend UHPCs containing fly ash and silica fume exhibited highest bulk properties.
- (2) The increase of aggregate-to-cementitious materials ratio (V_A/V_{cm}) from 0.80 to 1.20 resulted in reduced 28-day compressive strength of the studied UHPCs. However, reduction in compressive strength became less pronounced once curing age was extended to 90-day.
- (3) Cementitious materials types and compositions had more influence than aggregate-to-cementitious materials ratio on the strength properties of the studied UHPCs.
- (4) Inclusion of steel fibers significantly improved splitting-tensile resistance and flexural strength, whereas its effect on compressive strength and elastic modulus was minimal.
- (5) Straight steel fibers produced a slightly better bulk properties and dimensional stability than hooked fibers.
- (6) Drying shrinkage of the plain UHPCs decreased with increases in aggregate-to-cementitious materials ratios (V_A/V_{cm}). Secondary cementitious materials had significant effects on drying shrinkage of the studied UHPCs, with fly ash performing the best and silica fume performing the worst. Addition of fly ash or natural pozzolan and steel fibers compensated for the higher drying shrinkage exhibited by the silica fume in the binary blend UHPCs.
- (7) The studied plain UHPC beams failed in a brittle manner. A clear strain-hardening before peak strength was observed in steel fiber-reinforced UHPCs. An increase in steel fiber content significantly improved post-peak retention capacity of the studied fiber-reinforced UHPCs.

8. Data availability statement

Some or all data, models, or code that support the findings of this study are available from the corresponding author upon reasonable request.

CRedit authorship contribution statement

Ariful Hasnat: Methodology, Formal analysis, Data curation, Writing – original draft. **Nader Ghafoori:** Conceptualization, Supervision, Project administration.

Declaration of Competing Interest

The authors declare that they have no known competing financial interests or personal relationships that could have appeared to influence the work reported in this paper.

Acknowledgements

This study was funded by a grant made possible by the US Department of Transportation under the University Transportation Program (Grant No. GR09035). Thanks is extended to the funding agency and the suppliers who donated materials.

References

- [1] T.T.M. Ahlborn, D.K. Harris, D.L. Misson, E.J. Peuse, Characterization of strength and durability of ultra-high-performance concrete under variable curing conditions, *Transp. Res. Rec.* 2251 (1) (2011) 68–75.
- [2] K. Wille, A.E. Naaman, G.J. Parra-Montesinos, Ultra-High Performance Concrete with Compressive Strength Exceeding 150 MPa (22 ksi): A Simpler Way, *ACI Mater. J.* 108 (1) (2011) 46–54.
- [3] C. Wang, C. Yang, F. Liu, C. Wan, X. Pu, Preparation of ultra-high performance concrete with common technology and materials, *Cem. Concr. Compos.* 34 (4) (2012) 538–544.
- [4] C. Magureanu, I. Sosa, C. Negrutiu, B. Heghes, Mechanical properties and durability of ultra-high-performance concrete, *ACI Mater. J.* 109 (2) (2012) 177–183.
- [5] M.J. Lee, M.G. Lee, Y. Huang, K.L. Lee, UHPC precast concrete under severe freeze-thaw conditions, *Int. J. Eng. Technol.* 5 (4) (2013) 452.
- [6] M.o. Alkaysi, S. El-Tawil, Z. Liu, W. Hansen, Effects of silica powder and cement type on durability of ultra high performance concrete (UHPC), *Cem. Concr. Compos.* 66 (2016) 47–56.
- [7] Ç. Yağcınkaya, H. Yazıcı, Effects of ambient temperature and relative humidity on early-age shrinkage of UHPC with high-volume mineral admixtures, *Constr. Build. Mater.* 144 (2017) 252–259.
- [8] K. Ragalwar, W.F. Heard, B.A. Williams, R. Ranade, Significance of the particle size distribution modulus for strain-hardening-ultra-high performance concrete (SH-UHPC) matrix design, *Constr. Build. Mater.* 234 (2020) 117423, <https://doi.org/10.1016/j.conbuildmat.2019.117423>.
- [9] ACI Committee 239. (2018). Ultra-High-Performance Concrete: An Emerging Technology Report (ACI 239R-18). Farmington Hills, MI: American Concrete Institute..
- [10] ASTM C1856 / C1856M-17, Standard Practice for Fabricating and Testing Specimens of Ultra-High Performance Concrete, ASTM International, West Conshohocken, PA, 2017, www.astm.org..
- [11] P.Y. Blais, M. Couture, Precast, prestressed pedestrian bridge – world's first reactive powder concrete structure, *PCI journal* 44 (5) (1999) 60–71.
- [12] I.L. Larsen, R.T. Thorstensen, The influence of steel fibres on compressive and tensile strength of ultra high performance concrete: A review, *Constr. Build. Mater.* 256 (2020) 119459, <https://doi.org/10.1016/j.conbuildmat.2020.119459>.
- [13] R. Karim, M. Najimi, B. Shafei, Assessment of transport properties, volume stability, and frost resistance of non-proprietary ultra-high performance concrete, *Constr. Build. Mater.* 227 (2019) 117031, <https://doi.org/10.1016/j.conbuildmat.2019.117031>.
- [14] O. Bonneau, C. Vernet, M. Moranville, P.C. Attcin, Characterization of the granular packing and percolation threshold of reactive powder concrete, *Cem. Concr. Res.* 30 (12) (2000) 1861–1867.
- [15] S. Jacobsen, E.J. Sellevold, Self healing of high strength concrete after deterioration by freeze/thaw, *Cem. Concr. Res.* 26 (1) (1996) 55–62.
- [16] K. Tang, Stray current induced corrosion of steel fibre reinforced concrete, *Cem. Concr. Res.* 100 (2017) 445–456.
- [17] S.L. Yang, S.G. Millard, M.N. Soutsos, S.J. Barnett, T.T. Le, Influence of aggregate and curing regime on the mechanical properties of ultra-high performance fibre reinforced concrete (UHPFRC), *Constr. Build. Mater.* 23 (6) (2009) 2291–2298.
- [18] R. Zhong, K. Wille, R. Viegas, Material efficiency in the design of UHPC paste from a life cycle point of view, *Constr. Build. Mater.* 160 (2018) 505–513.
- [19] C.M. Tam, V.W.Y. Tam, K.M. Ng, Assessing drying shrinkage and water permeability of reactive powder concrete produced in Hong Kong, *Constr. Build. Mater.* 26 (1) (2012) 79–89.
- [20] M.G. Sohail, B. Wang, A. Jain, R. Kahraman, N.G. Ozerkan, B. Gencturk, M. Dawood, A. Belarbi, Advancements in concrete mix designs: High-performance and ultrahigh-performance concretes from 1970 to 2016, *J. Mater. Civ. Eng.* 30 (3) (2018) 04017310, [https://doi.org/10.1061/\(ASCE\)MT.1943-5533.0002144](https://doi.org/10.1061/(ASCE)MT.1943-5533.0002144).
- [21] Acker, P., & Behloul, M. (2004, September). Ductal® technology: A large spectrum of properties, a wide range of applications. In Proc. of the Int. Symp. on UHPC Kassel, Germany (pp. 11–23)..
- [22] M. Schmidt, E. Fehling, Ultra-high-performance concrete: research, development and application in Europe, in: 7th International Symposium on the Utilization of High-Strength- and High-Performance-Concrete, ACI Washington, 2005, SP.228-4, pp. 51–78..
- [23] Graybeal, B. UHPC in the U.S. highway transportation system, in: Proceedings of the Second International Symposium on Ultra High Performance Concrete, Kassel University Press GmbH, Kassel, Germany, 2008, p. 11..
- [24] A. Arora, A. Almajiddidi, F. Kianmofrad, B. Mobasher, N. Neithalath, Material design of economical ultra-high performance concrete (UHPC) and evaluation of their properties, *Cem. Concr. Compos.* 104 (2019) 103346, <https://doi.org/10.1016/j.cemconcomp.2019.103346>.
- [25] R. Yang, R. Yu, Z. Shui, X. Gao, X. Xiao, X. Zhang, Y. Wang, Y. He, Low carbon design of an Ultra-High Performance Concrete (UHPC) incorporating phosphorous slag, *J. Cleaner Prod.* 240 (2019) 118157, <https://doi.org/10.1016/j.jclepro.2019.118157>.
- [26] A. Alsalmán, C.N. Dang, W. Micah Hale, Development of ultra-high performance concrete with locally available materials, *Constr. Build. Mater.* 133 (2017) 135–145.
- [27] Y.-W. Chan, S.-H. Chu, Effect of silica fume on steel fiber bond characteristics in reactive powder concrete, *Cem. Concr. Res.* 34 (7) (2004) 1167–1172.
- [28] Graybeal, B. (2006). Material property characterization of ultra-high performance concrete. FHWA, US Department of Transportation. Report No. FHWA-HRT-06-103, McLean, VA..
- [29] P. Ganesh, A.R. Murthy, Tensile behaviour and durability aspects of sustainable ultra-high performance concrete incorporated with GGBS as cementitious material, *Constr. Build. Mater.* 197 (2019) 667–680.
- [30] W. Meng, M. Valipour, K.H. Khayat, Optimization and performance of cost-effective ultra-high performance concrete, *Mater. Struct.* 50 (29) (2017), <https://doi.org/10.1617/s11527-016-0896-3>.

- [31] S. Abbas, A.M. Soliman, M.L. Nehdi, Exploring mechanical and durability properties of ultra-high performance concrete incorporating various steel fiber lengths and dosages, *Constr. Build. Mater.* 75 (2015) 429–441.
- [32] P. Máca, R. Sovják, T. Vavřínek, Experimental investigation of mechanical properties of UHPFRC, *Procedia Eng.* 65 (2013) 14–19.
- [33] D.-Y. Yoo, H.-O. Shin, J.-M. Yang, Y.-S. Yoon, Material and bond properties of ultra high performance fiber reinforced concrete with micro steel fibers, *Compos. B Eng.* 58 (2014) 122–133.
- [34] K. Wille, D.J. Kim, A.E. Naaman, Strain-hardening UHP-FRC with low fiber contents, *Mater. Struct.* 44 (3) (2011) 583–598.
- [35] Z. Wu, C. Shi, W. He, L. Wu, Effects of steel fiber content and shape on mechanical properties of ultra high performance concrete, *Constr. Build. Mater.* 103 (2016) 8–14.
- [36] S.H. Park, D.J. Kim, G.S. Ryu, K.T. Koh, Tensile behavior of ultra high performance hybrid fiber reinforced concrete, *Cem. Concr. Compos.* 34 (2) (2012) 172–184.
- [37] D.J. Kim, S.H. Park, G.S. Ryu, K.T. Koh, Comparative flexural behavior of hybrid ultra high performance fiber reinforced concrete with different macro fibers, *Constr. Build. Mater.* 25 (11) (2011) 4144–4155.
- [38] A.M.T. Hassan, S.W. Jones, G.H. Mahmud, Experimental test methods to determine the uniaxial tensile and compressive behaviour of ultra high performance fibre reinforced concrete (UHPFRC), *Constr. Build. Mater.* 37 (2012) 874–882.
- [39] B.-I. Bae, H.-K. Choi, C.-S. Choi, Flexural strength evaluation of reinforced concrete members with ultra high performance concrete, *Adv. Mater. Sci. Eng.* 2016 (2016) 1–10, <https://doi.org/10.1155/2016/2815247>.
- [40] ASTM A820 / A820M-16, Standard Specification for Steel Fibers for Fiber-Reinforced Concrete, ASTM International, West Conshohocken, PA, 2016, www.astm.org.
- [41] ASTM C230 / C230M-14, Standard Specification for Flow Table for Use in Tests of Hydraulic Cement, ASTM International, West Conshohocken, PA, 2021, www.astm.org.
- [42] J.E. Funk, D.R. Dinger, Predictive process control of crowded particulate suspensions, applied to ceramic manufacturing, Kluwer Academic Publishers, Boston, USA, 1994.
- [43] ASTM C29 / C29M-17a, Standard Test Method for Bulk Density ("Unit Weight") and Voids in Aggregate, ASTM International, West Conshohocken, PA, 2017, www.astm.org.
- [44] ASTM C642-13, Standard Test Method for Density, Absorption, and Voids in Hardened Concrete, ASTM International, West Conshohocken, PA, 2013, www.astm.org.
- [45] ASTM C39 / C39M-20, Standard Test Method for Compressive Strength of Cylindrical Concrete Specimens, ASTM International, West Conshohocken, PA, 2020, www.astm.org.
- [46] ASTM C496 / C496M-17, Standard Test Method for Splitting Tensile Strength of Cylindrical Concrete Specimens, ASTM International, West Conshohocken, PA, 2017, www.astm.org.
- [47] ASTM C596-18, Standard Test Method for Drying Shrinkage of Mortar Containing Hydraulic Cement, ASTM International, West Conshohocken, PA, 2018, www.astm.org.
- [48] ASTM C1609 / C1609M-19a, Standard Test Method for Flexural Performance of Fiber-Reinforced Concrete (Using Beam With Third-Point Loading), ASTM International, West Conshohocken, PA, 2019, www.astm.org.
- [49] ASTM C469 / C469M-14, Standard Test Method for Static Modulus of Elasticity and Poisson's Ratio of Concrete in Compression, ASTM International, West Conshohocken, PA, 2014, www.astm.org.
- [50] B.W. Langan, K. Weng, M.A. Ward, Effect of silica fume and fly ash on heat of hydration of Portland cement, *Cem. Concr. Res.* 32 (7) (2002) 1045–1051.
- [51] M. Jalal, A. Pouladkhan, O.F. Harandi, D. Jafari, Comparative study on effects of Class F fly ash, nano silica and silica fume on properties of high performance self compacting concrete, *Constr. Build. Mater.* 94 (2015) 90–104.
- [52] T. Chen, X. Gao, M. Ren, Effects of autoclave curing and fly ash on mechanical properties of ultra-high performance concrete, *Constr. Build. Mater.* 158 (2018) 864–872.
- [53] F.U. Shaikh, T. Nishiwaki, S. Kwon, Effect of fly ash on tensile properties of ultra-high performance fiber reinforced cementitious composites (UHP-FRCC), *J. Sustainable Cement-Based Mater.* 7 (6) (2018) 357–371.
- [54] H. Yazıcı, E. Deniz, B. Baradan, The effect of autoclave pressure, temperature and duration time on mechanical properties of reactive powder concrete, *Constr. Build. Mater.* 42 (2013) 53–63.
- [55] P.K. Mehta, P.J. Monteiro, Concrete Microstructure, Properties and Materials, (3rd ed.), McGraw Hill, 2005.
- [56] N.N. Gerges, C.A. Issa, S. Fawaz, Effect of construction joints on the splitting tensile strength of concrete, *Case Stud. Constr. Mater.* 3 (2015) 83–91.
- [57] Van Quan H., Van Tuoi N., Nguyen C.V. (2020) Effect of fly ash on the mechanical properties and drying shrinkage of the cement treated aggregate crushed stone. In: Ha-Minh C., Dao D., Benboudjema F., Derrible S., Huynh D., Tang A. (eds) CIGOS 2019, Innovation for Sustainable Infrastructure. Lecture Notes in Civil Engineering, vol 54. Springer, Singapore. https://doi.org/10.1007/978-981-15-0802-8_65.
- [58] A. Le Hoang, E. Fehling, Influence of steel fiber content and aspect ratio on the uniaxial tensile and compressive behavior of ultra high performance concrete, *Constr. Build. Mater.* 153 (2017) 790–806.
- [59] J.J. Park, D.Y. Yoo, G.J. Park, S.W. Kim, Feasibility of reducing the fiber content in ultra-high-performance fiber-reinforced concrete under flexure, *Materials* 10 (2) (2017) 118, <https://doi.org/10.3390/ma10020118>.
- [60] H.R. Sobuz, P. Visintin, M.S. Mohamed Ali, M. Singh, M.C. Griffith, A.H. Sheikh, Manufacturing ultra-high performance concrete utilising conventional materials and production methods, *Constr. Build. Mater.* 111 (2016) 251–261.